ChemMedChem

Review
doi.org/10.1002/cmdc.202300099

Chemistry Europe
European Chemical Societies Publishing

www.chemmedchem.org

DprE1 Inhibitors: Enduring Aspirations for Future Antituberculosis Drug Discovery

Saloni Yadav,[a] Aastha Soni,[a] Omprakash Tanwar,*[a] Rajendra Bhadane,*[b, d] Gurdyal S. Besra,[c] and Neha Kawathekar[a]

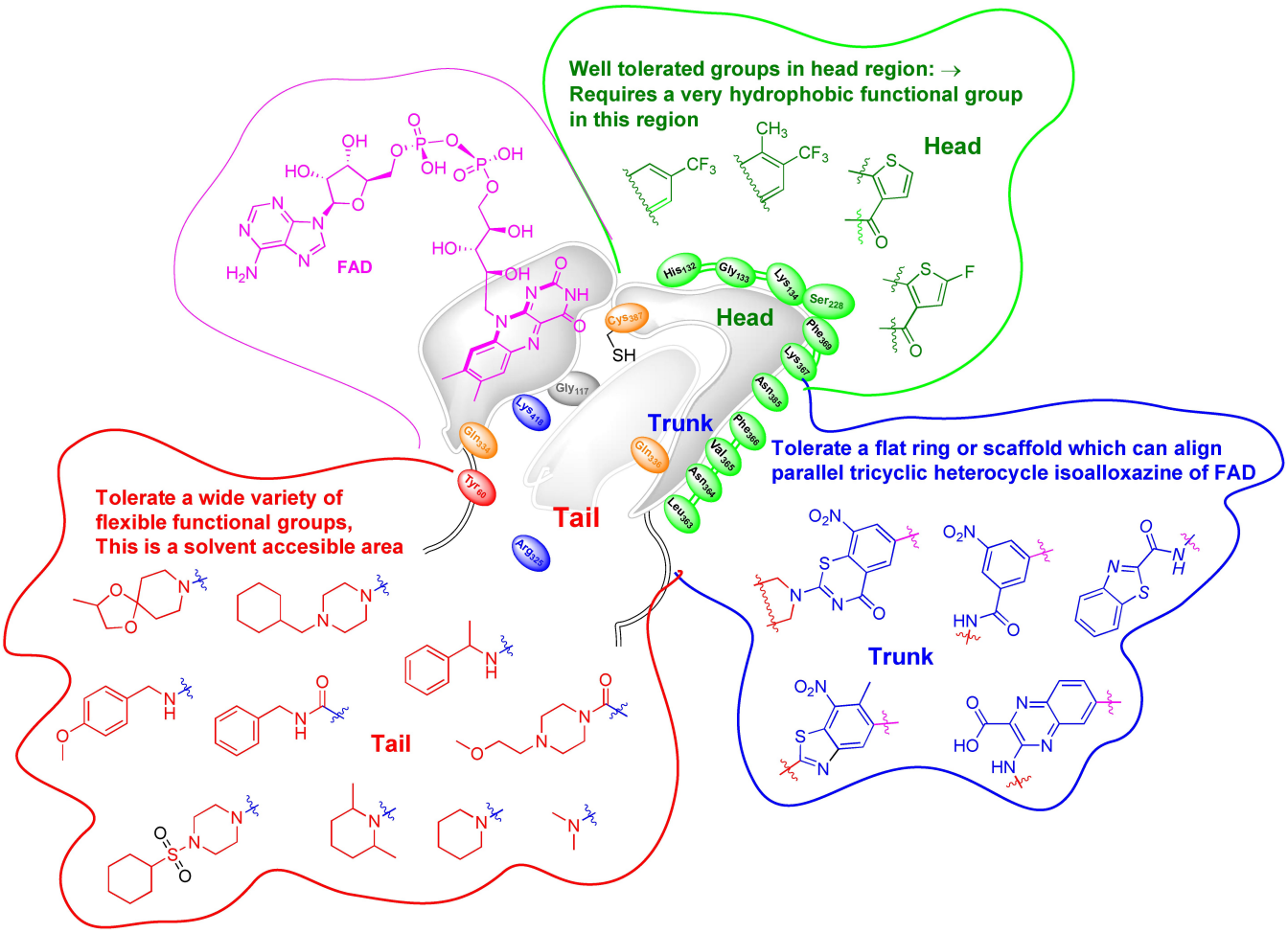

DprE1 is a crucial enzyme involved in the cell wall synthesis of *Mycobacterium tuberculosis* and a promising target for anti-tuberculosis drug development. However, its unique structural characteristics for ligand binding and association with DprE2 make developing new clinical compounds challenging. This review provides an in-depth analysis of the structural requirements for both covalent and non-covalent inhibitors, their 2D and 3D binding patterns, as well as their biological activity data in vitro and in vivo, including pharmacokinetic information. We also introduce a protein quality score (PQS) and an active-site map of the DprE1 enzyme to help medicinal chemists better understand DprE1 inhibition and develop new and effective anti-TB drugs. Furthermore, we examine the resistance mechanisms associated with DprE1 inhibitors to understand future developments due to resistance emergence. This comprehensive review offers insight into the DprE1 active site, including protein-binding maps, PQS, and graphical representations of known inhibitors, making it a valuable resource for medicinal chemists working on future antitubercular compounds.

Introduction

Tuberculosis (TB) remains one of the top ten leading causes of death worldwide, particularly in low-income countries. According to the WHO's 2020 report, 1.4 million people died from TB in 2019.[1] Although treatment is available, its success rate is only 57% due to the lengthy and costly regimens.[1] The emergence of extensively drug-resistant (XDR) TB strains has further increased the cost of treatment.[2] TB drug resistance has developed through mechanisms such as efflux,[3] genetic mutations,[4] deficient DNA repair, and compensatory evolution.[5] The low permeability of the TB cell wall, slow growth, dormancy, drug tolerance, and persistence present challenges for the discovery of new TB drugs.[6]

Many adverse effects are associated with the use of first-line anti-TB drugs, such as hepatitis, cutaneous reactions, haematological reactions, gastrointestinal intolerance, and renal failure.[7] Additionally, the high lipophilicity requirement of compounds to inhibit *Mtb* growth restricts the development of novel and diverse anti-TB hits/leads and impedes their optimization of physicochemical properties.[6,8] In light of this, understanding the metabolic pathways involved in *Mtb* and optimizing the absorption, distribution, metabolism, excretion, and toxicity (ADMET) of small molecules is crucial. This emphasizes the need for the discovery of faster-acting and safer drugs for future use.[9]

Several excellent reviews on anti-tubercular (anti-TB) drug discovery have been published.[6,10] Most anti-TB drugs target *Mtb* cell wall assembly, including mycolic acid biosynthesis (isoniazid/ethionamide) and arabinogalactan/lipoarabinomannan biosynthesis (ethambutol). The importance of the physicochemical properties of drugs and *Mtb* transporters in the discovery of new anti-TB medicines has been nicely explained by Elizabeth and Robert.[11]

Decaprenylphosphoryl-β-D-ribose-2′-epimerase oxidase (DprE1, Rv-3790) and decaprenylphosphoryl-β-D-ribose-2′-epimerase (DprE2, Rv-3791) play a crucial role in the synthesis of the arabinan components of arabinogalactan (AG) and lipoarabinomannan (LAM).[12]

DprE1 and DprE2 are highly conserved in *Mtb* and are essential for cell wall biosynthesis. DprE1 has sometimes been referred to as a "magic drug target" and is the focus of intense TB drug discovery efforts.[12b] Many excellent reviews have been published elsewhere, highlighting the importance and utility of DprE1 inhibitors in the development of different anti-TB hits and leads[13] Emphasizing the rich chemical diversity of DprE1 inhibitors will serve as the foundation for future anti-TB drug discovery.

Significance of DprE1 in *Mtb* Cell Wall Synthesis and Its Mechanism of Inhibition

The *Mtb* cell wall consists of three essential components: the long-chain mycolic acids (MA) located at the non-reducing termini of the highly branched AG, which is linked to peptidoglycan (PG) through a linker unit, and the essential LAM polysaccharide located in the mycobacterial outer membrane.[14]

The arabinan components of AG and LAM are exclusively synthesized by distinct arabinofuranosyl transferases using the common decaprenylphosphoryl-β-D-arabinofuranose (DPA) (**3**) sugar donor found in *Mtb*. The biosynthesis of DPA (**3**) begins with activation of ribose-5-phosphate by phosphoribosyl-1-pyrophosphate synthetase (PrsA, Rv1017c) to form 5-phosphoribosyl-1-pyrophosphate (pRpp). Decaprenyl monophosphate is then linked to pRpp using UbiA (Rv3806c) to produce decaprenylphosphoryl-5-phosphoribose (DPPR), which is then dephosphorylated by Rv3807c to form decaprenyl-5-phosphoribose (DPR, **1**). DPA (**3**) is then synthesized from DPR (**1**) in two steps: the conversion of DPR (**1**) to decaprenylphosphoryl-2-ketoribose (DPX, **2**) by the flavoprotein enzyme DprE1 (Rv-3790), and the conversion of DPX (2)

[a] *S. Yadav, A. Soni, Dr. O. Tanwar, Dr. N. Kawathekar*
Department of Pharmacy
Shri Govindram Seksaria Institute of Technology and Science
23-Park Road, Indore, Madhya Pradesh (India)
E-mail: op0816@gmail.com
[b] *Dr. R. Bhadane*
Turku Cellular Microbiology Laboratory (TCML)
Åbo Akademi University, 20014 Turku (Finland)
[c] *Prof. G. S. Besra*
Institute of Microbiology and Infection, School of Biosciences
University of Birmingham, Edgbaston, Birmingham, B15 2TT (UK)
[d] *Dr. R. Bhadane*
Institute of Biomedicine, University of Turku, 20520 Turku (Finland)

to DPA (3) by the NADH-dependent reductase DprE2 (Rv3791) (Figure 1).[12b,15]

The DprE1 and DprE2 enzymes work together to convert DPR (1) to DPA (3), which is an essential precursor for AG and LAM biosynthesis. In 2009, Makarov *et al.*,[16] discovered the first series of DprE1 inhibitors, referred to as Benzothiazinones (BTZs). Since then, several additional DprE1 inhibitors, including the clinical candidate Macozinone or PBTZ169, have been identified, but none of them are currently available for clinical use. Our aim is to provide the latest information on each aspect of this research, and as a result, the present review highlights the significance of DprE1 as a target in the search for new tuberculosis drugs.

Structural insights into the DprE1 active site

To date, there are 31 DprE1 structures reported in the PDB from *Mtb* and *Mycobacterium smegmatis* (*Msm*), with both species sharing 83% sequence identity and RMSD of 0.464 Å.[17] From these 27 PDBs are for *Mtb*(4FEH,[13e] 4FDN,[13e] 4FDO,[13e] 4FDP,[13e] 4FF6,[13e] 4KW5,[18] 4NCR,[19] 4P8H(not published), 4PFD(not published), 4PFA(not published), 4P8K,[20] 4P8L,[20] 4P8C,[20] 4P8T,[20] 4P8Y,[20] 4P8M,[20] 4P8N,[20] 4P8P,[20] 5OEP,[21] 5OEL,[21] 5OEQ,[21] 6G83,[22] 6HEZ,[23] 6HFW,[23] 6HFV,[23] 6HF0[23] and 6HF3[23]) while four PDBs for *Msm*(4AUT,[24] 4F4Q,[24] 4G3T,[25] and 4G3U[25]). The FAD bound $DprE1_{TB}$ apo-proteins are also published as 4FDP[13e] (monoclinic crystal form) and 4FEH (not published, hexagonal crystal form), while specific $DprE1_{SM}$ apo-proteins are published as 4G3 U[25] (monoclinic crystal form) and 4G3T[25] (hexagonal crystal form). The complete information regarding protein structure resolution, ligands, and overall protein quality score of these PDBs are mentioned in Table 1.

Based on the overall quality of PDB structures, we have formulated a general Protein Quality Score (PQS) for each entry so that the researchers can choose the protein of interest for their molecular modeling studies. The PQS is a coarse quality score for a PDB entry inspired by many factors, such as resolution, presence or absence of missing loops/

Saloni Yadav holds a master's degree in Pharmacy from Shri G.S. Institute of Technology and Science, Indore, which she completed in 2021. Currently, she is employed as an Assistant Professor at Indore Institute of Pharmacy in Indore. Her area of research focuses on computer-aided design and synthesis, and she has expertise in molecular docking and virtual screening of small molecules using the GLIDE software. She has presented her research at several national and international conferences.

Aastha Soni earned her Master of Pharmacy degree with a focus in Medicinal and Pharmaceutical Chemistry from Shri Govindram Seksaria Institute of Technology and Science in Indore, India. During her studies, she focused on the design and synthesis of anti-diabetic agents based on 1,2,3-triazoles. Her research interests lie in the fields of computational and medicinal chemistry. Currently, she works as a Pharmacovigilance Assistant at Elite Safety Sciences in Gurugram, India.

Dr. Omprakash Tanwar is a seasoned medicinal chemist with 13+ years of experience in the industry. He boasts a strong foundation in bioorganic chemistry and molecular modeling and is renowned for his proficiency in creating new antimicrobial agents. He recently finished a five-month SIRE fellowship at the University of Oxford and has an impressive publication record, with over 20 research papers and two patents to his name. Currently, he serves as an Assistant Professor at the Department of Pharmacy at SHRI G. S. INSTITUTE OF TECHNOLOGY & SCIENCE in Indore, where he is dedicated to furthering the field of medicinal chemistry through his research and teaching

Dr. Rajendra Bhadane is a senior researcher at the Turku Cellular Microbiology Laboratory (TCML) within the Institute of Biomedicine at the University of Turku. His expertise includes virtual screening and chemoinformatics, structure-based and ligand-based drug design, molecular dynamics simulations of protein-ligand complexes, nanoparticle and polymer modeling, DFT calculations of small molecules, and various protein-related techniques such as expression, purification, stability analysis, and crystallization. He also has experience in small molecule and oligonucleotide synthesis, characterization using FTIR, NMR, and mass spectrometry, and nanoparticle fabrication. In addition to his research background, he has taught for 8 years at the undergraduate level.

As the head of a top-tier, multidisciplinary team, Dr. Gurdyal S. Besra leads studies on the physiology of the Mycobacterium tuberculosis cell wall and the possibilities of iNKT/CD1d therapies. He has received and efficiently overseen over 50 research grants, valued at more than £35 million, from esteemed organizations such as The Wellcome Trust, the Biotechnology and Biological Sciences Research Council (BBSRC), and the Medical Research Council (MRC).

Dr. Neha Kawathekar has extensive experience in both teaching and research, having spent over two decades in the field. She focuses on discovering new antimalarial and antitubercular agents and has published numerous articles in reputable journals and presented her work at both national and international events. In addition to her research, she has mentored many PhD and master's students and has expertise in teaching medicinal chemistry and drug design.

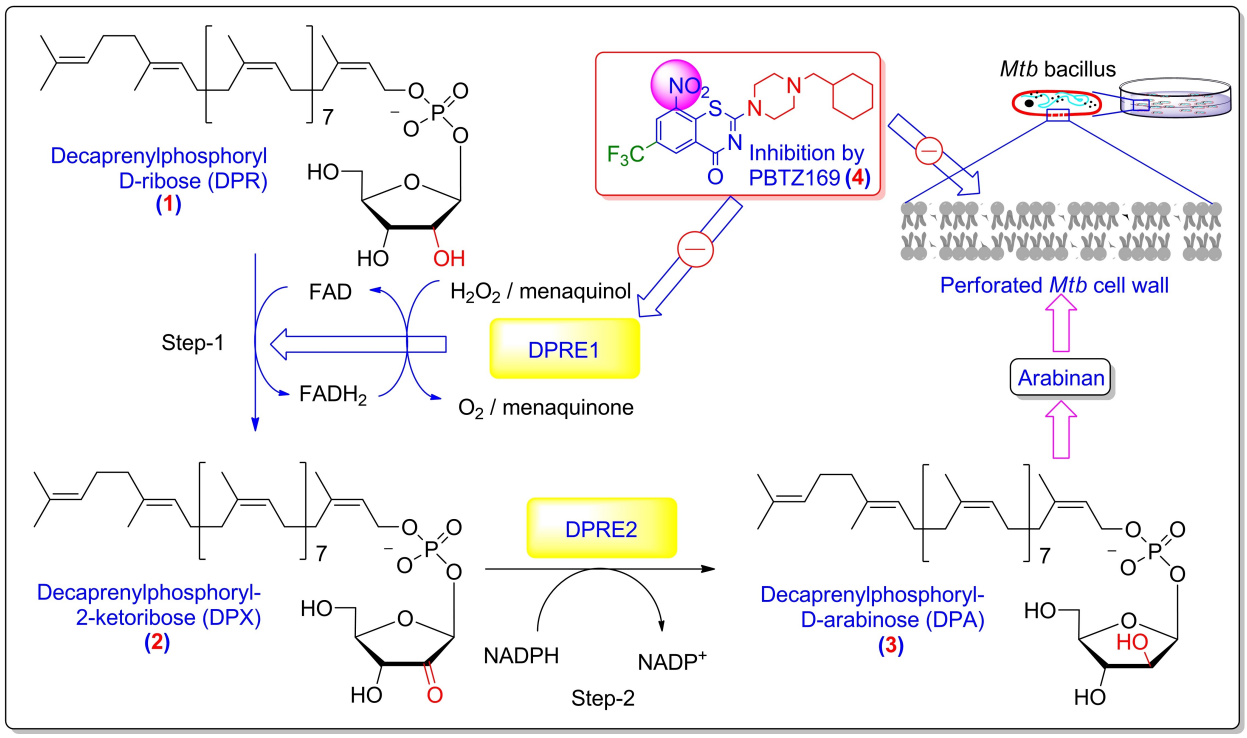

Figure 1. The role of DprE1 in the biosynthesis of the *Mycobacterium tuberculosis* (*Mtb*) cell wall (arabinan) and its inhibition by the DprE1 inhibitor macozinone (PBTZ169, **4**).

outliers, and the number of times a PDB appeared in the literature.

DprE1 contains two domains of a vanillyl-alcohol oxidase and belongs to the family of oxidoreductases, which includes both the FAD-binding domain (consisting of amino acid residues 7–196 and 413–461) and the substrate/inhibitor-binding domain (comprising amino acid residues 197–412). The FAD is buried within the FAD-binding domain, with the isoalloxazine of FAD located at the junction between the substrate/inhibitor-binding domain. The FAD is essential for the protein's proper functioning.[17] The electron density map of all crystal forms shows disorderliness in two surface loops within the substrate/inhibitor-binding domain. Loop I (residues 269–303) and loop II (residues 316–330) are situated above the substrate/inhibitor-binding domain and facilitate the attachment of the ligand to the substrate/inhibitor-binding site. The behavior of these loops varies depending on the bound inhibitors. Some inhibitors, such as Ty38C (5), QN118 (6), and QN127 (7), stabilize loop I, while CT319 (13) stabilizes loop II, and Ty36C (20) and QN129 (8) stabilize both loops (Figure 2).[17]

Binding Site Analysis of DprE1

Several reports on the structure of the DprE1 protein and its active site have been published by Piton *et al.*[17] and by Chikhale *et al.*.[13a] Since then, nine new PDB structures of DprE1 have been deposited in the PDB database. However, a comprehensive analysis of these structures is still necessary. With sufficient data now available, it is possible to perform a more in-depth analysis of the active site and gain a better understanding of how DprE1 can bind both covalent and non-covalent inhibitors. Our analysis of the DprE1 binding site has divided it into head, trunk, and tail regions based on the conformations of the co-crystallized ligands. In all PDB structures, the FAD is positioned in a fixed location within the binding pocket and serves as a support for ligand binding (Figure 3).

The head region

The head region of the active site is composed of a hydrophobic cavity formed by His132, Gly133, Lys134, Ser228, Lys367, Phe369, and Asn385. The cavity is more or less identical in the X-ray structures, but it may have moved to accommodate the inhibitors. The occupancy of this region governs the inhibitory activity of DprE1. If ligands completely occupy the head region, they strongly influence the ligand-receptor affinity, i.e., pBTZ169 (**4**) and BTZ043 (**9**). Both ligands contain a -CF_3 group, an ideal feature for this cavity, and pack very well in this region by forming dense Vander Waals interactions with the backbone of residues His132, Gly133, and Lys134.[13e] Probably, the early structure-activity relationship (SAR) for BTZs favored the inclusion of a CF3 group in this position. Therefore, most of the ligands reported in the literature contain a CF_3 group occupying the

Table 1. Information on reported DprE1 PDB crystal structures and their protein quality score (PQS).[a]

PDB code (resolution [Å])	Ligand name	Ligand structure	PQS (out of five)	Integrity of side chains and status of missing residues Use in molecular modeling (MM) studies	Ref.
PDB entries with covalent DprE1 inhibitors					
4NCR (1.88)	PBTZ169 (**4**)	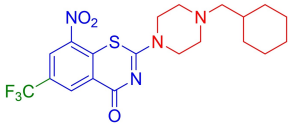		Missing residues in both chains A and B. Used one MM study.	[19,29a]
4F4Q (2.62)	BTZ043 (**9**)	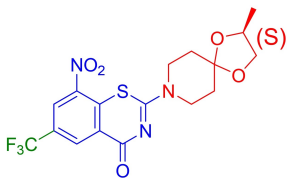		Missing residues in both chains A and B. Not used in any virtual screening.	[24]
4PFA (2.56)	BTO (**10**)	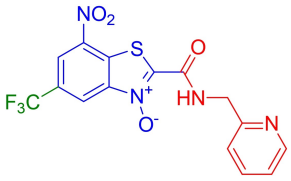		–	[20]
4P8H (3.00)	CBT-37 (**11**)	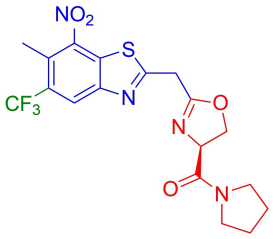		Missing residues in both chains A and B. Many outliers are present in the side chains. Used in one MM study.	[29a,49]
4FF6 (2.60)	CT325 (**12**)	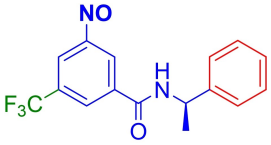		–	[13e]
4FDN (2.6)	CT325 (**12**)	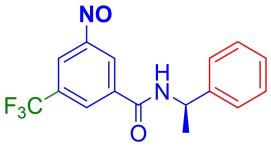		–	[13e,36]
4FDO (2.4)	CT319 (**13**)			Missing residues in the active site (269–297) and creating a closed-form. 4FDO appeared in six MM studies.	[13e,36,50,56–57,70,74,77]
6G83 (2.40)	sPBTZ169 (**14**)	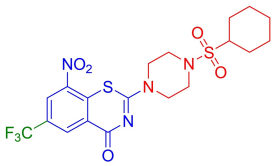		Missing residues in chain-A. Not used in any virtual screening.	[22,36]
6HEZ (2.30)	BTZ043 (**9**)	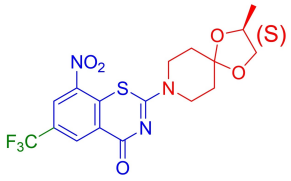		Missing residues in chain-A. Some side chain outliers are present. Not used in any virtual screening.	[23]

Table 1. continued

PDB code (resolution [Å])	Ligand name	Ligand structure	PQS (out of five)	Integrity of side chains and status of missing residues Use in molecular modeling (MM) studies	Ref.
PDB entries with covalent DprE1 inhibitors					
6HFW (2.47)	CMP1 (**15**)	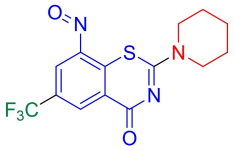		Missing residues in chain A. Not used in any virtual screening.	[23]
6HFV (2.05)	CMP2 (**16**)	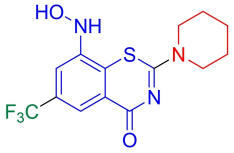		–	[23]
6HF0 (2.38)	Nitrobenzoxacine (**17**)	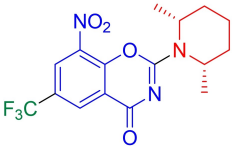		–	[23]
6HF3 (2.20)	Nitrobenzoxacine (**18**)	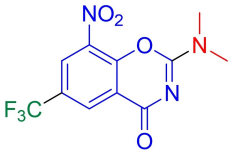		Many side-chain outliers are present, and missing residues are also present. In PDB 2D structure shows PBTZ169 bound, but compound (**18**) is attached.	[23]
PDB entries with non-covalent DprE1 inhibitors					
4PFD (2.30)	CBT-18 (**19**)	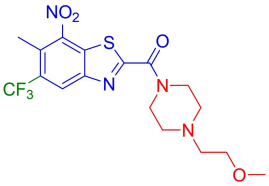		Missing residues in both chains A and B. fewer outliers are present in the side chain, Not used in any MM study	[49]
4P8K (2.49)	Ty38c (**5**)	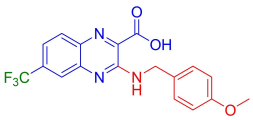		Missing residues in both chains, creating an open-form of the enzyme. 4P8K appeared in one MM study.	[20,78]
4P8C (1.95)	QN127 (**7**)	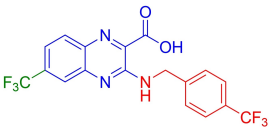		Missing residues in both chains. Many outliers are present in the side chain. It is not used in any virtual screening.	[20]
4P8L (2.02)	Ty36C (**20**)	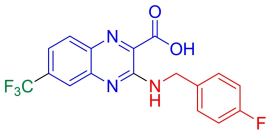		No missing residue in chain-A, but some are missing in chain-B. Some outliers are present Not used in any virtual screening but can be used as the chain-A has no missing residue and has good resolution. Extra ligand (2J3) is bound, which makes the active site a little larger. May give a clue for accommodating different ligands	[20]
4P8M (2.09)	QN114 (**21**)	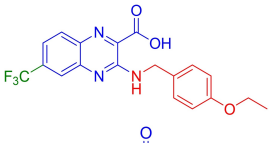		Missing residues in both chains. Some outliers are present Not used in any virtual screening.	[20]
4P8N (1.79)	QN118 (**6**)	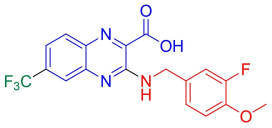		Missing residues in both chains. Many outliers are present. This PDB is not used in any virtual screening. Two conformations of ligands are visible in the PDB structure	[20]

Table 1. continued

PDB code (resolution [Å]) PDB entries with covalent DprE1 inhibitors	Ligand name	Ligand structure	PQS (out of five)	Integrity of side chains and status of missing residues Use in molecular modeling (MM) studies	Ref.
4P8P (2.2)	QN124 (**22**)	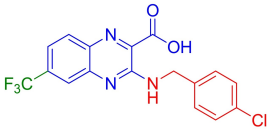		Missing residues in both chains. Many outliers are present. This PDB is not used in any virtual screening.	[20]
4P8Y (2.01)	The ester ofTy38c (**5**) is reported	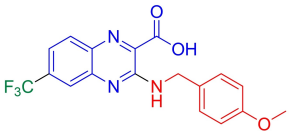		–	[20]
4P8T (2.55)	QN129 (**8**)	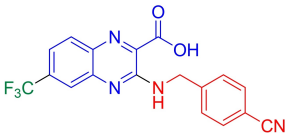		Same as 4P8L accept its resolution little less than 4P8L	[20]
4KW5 (2.61)	TCA1(**23**)	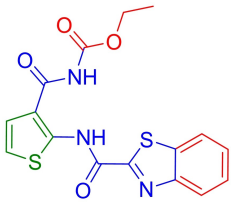		Missing residues in both chains and creating an open-form of the active site. Used in four MM studies	[18,56–57,79]
5OEP (2.35)	TCA481 (**24**)	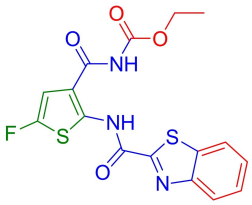		Missing loops are present in chain-A Not used in any virtual screening	[21]
5OEL (2.20)	TCA1(**23**)	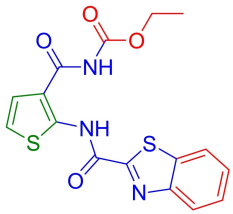		Many side-chain outliers are present, missing residues in chains. Mutant structure not suitable for VS, as it contains mutant Y314C.	[21]
5OEQ (2.25)	TCA020 (**25**)	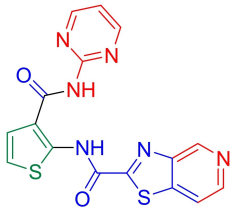		Missing residues in chain-A. Some side chain outliers are present. Not used in any virtual screening.	[21]

[a] Comparison of PDB structures by quality. Pie charts show the distribution of PDB structures based on their quality, as determined by a combination of PDB data and information from the literature. The green portion represents the percentage of structures with higher quality, while the red portion represents the percentage of structures with lower quality. The higher number of green portions in a pie represents better PDB structure.

head region, with the exception of a few ligands such as TCA1 (23). (see Figure 15A below). As buried hydrophobic interactions generally contribute to the stability of protein-ligand interactions and favor the ligand's increased affinity, the head region is the main driving force for drug-receptor interaction and its association with DprE1 [27] (see Figure 3). The sub-structures of the most often used hydrophobic scaffolds in many DprE1 inhibitors are given in (Figure 4). These structural motifs accommodate very well in the head region and can be incorporated into new ligands to achieve desired potency against DprE1.

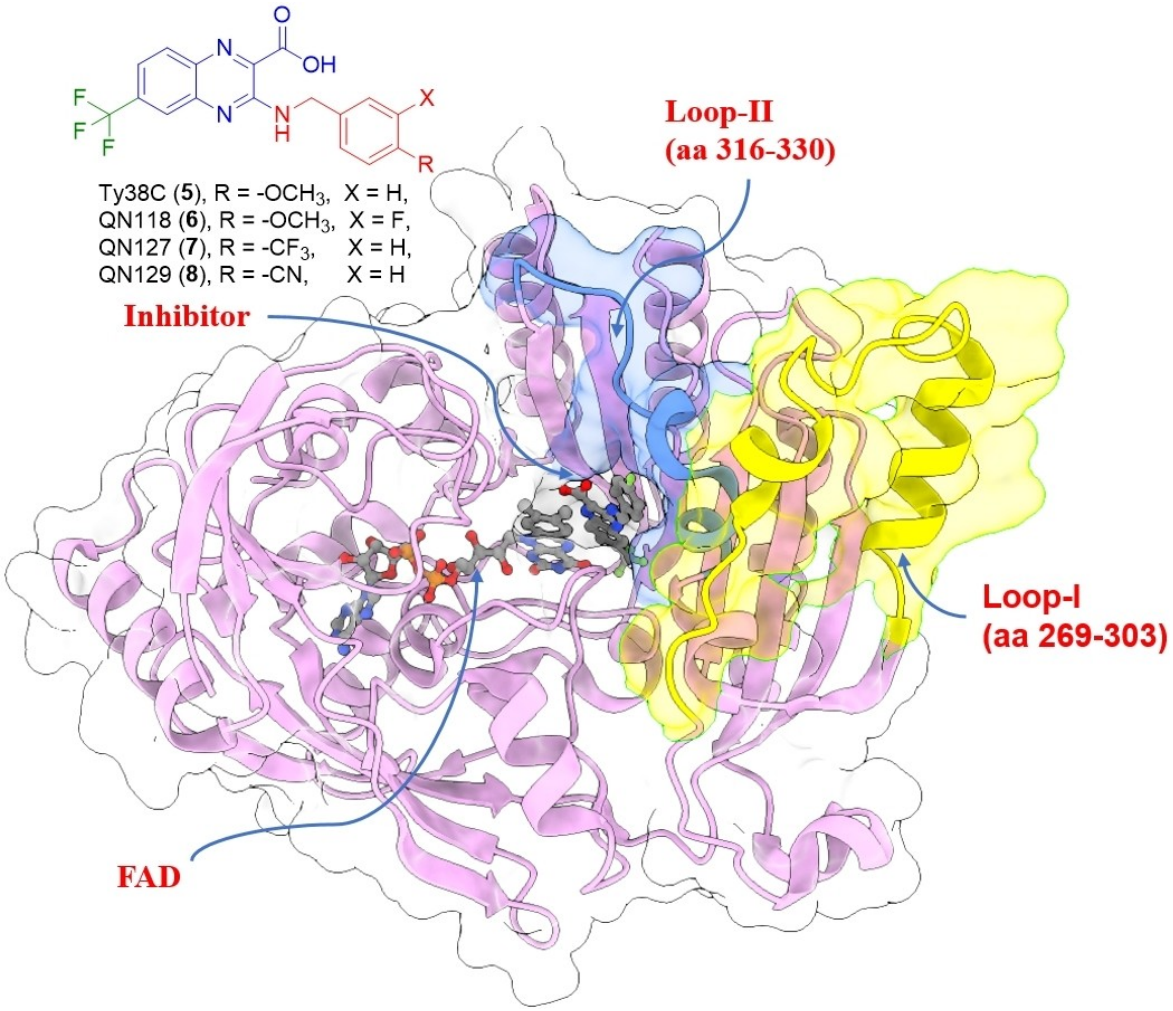

Figure 2. Depiction of the disordered loops of DprE1's substrate/inhibitor-binding and FAD-binding domains in the active site is shown (Loop-I is represented by amino acids 269–303 in yellow cartoon and by surface representation in blue, Loop-II is represented by amino acids 316–330 in blue surface representation; FAD and the ligand are shown in elemental ball and stick representation, while the rest of the protein is depicted in pink cartoon with a transparent white surface; the PDB ID is 4P8L[20]).

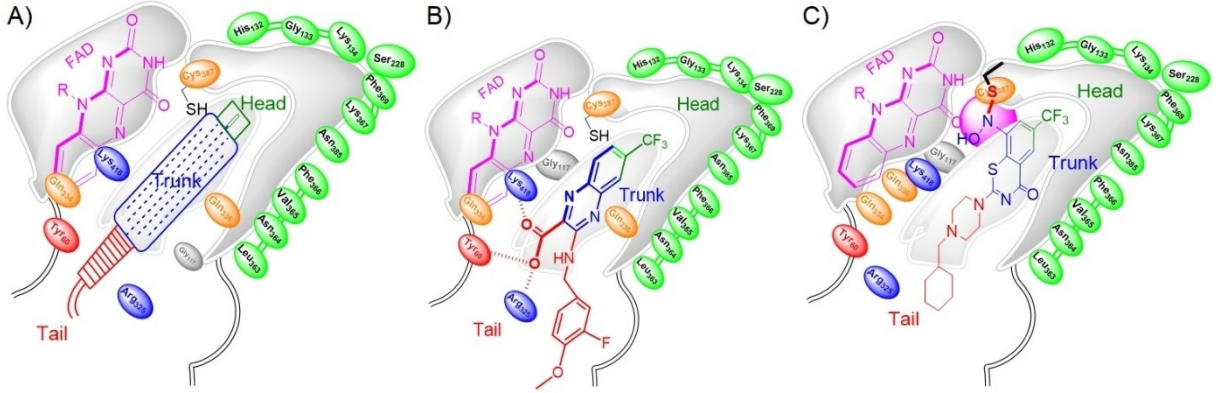

Figure 3. The map of the DprE1 active site is presented. A) A dummy model of the active site, which is divided into three regions: the head, trunk, and tail. B) A non-covalently bound inhibitor and its position within the active site. C) A covalently bound inhibitor and its placement in the active site. The green represents the hydrophobic (head) region, the blue represents the groups facing the FAD (trunk part), and red represents the solvent-accessible (tail) region. The electrophilic warhead is shown above the pink sphere. (B) The mechanism of Nitroso-activation (32) of BTZ derivatives and the formation of the Meisenheimer complex is also shown.

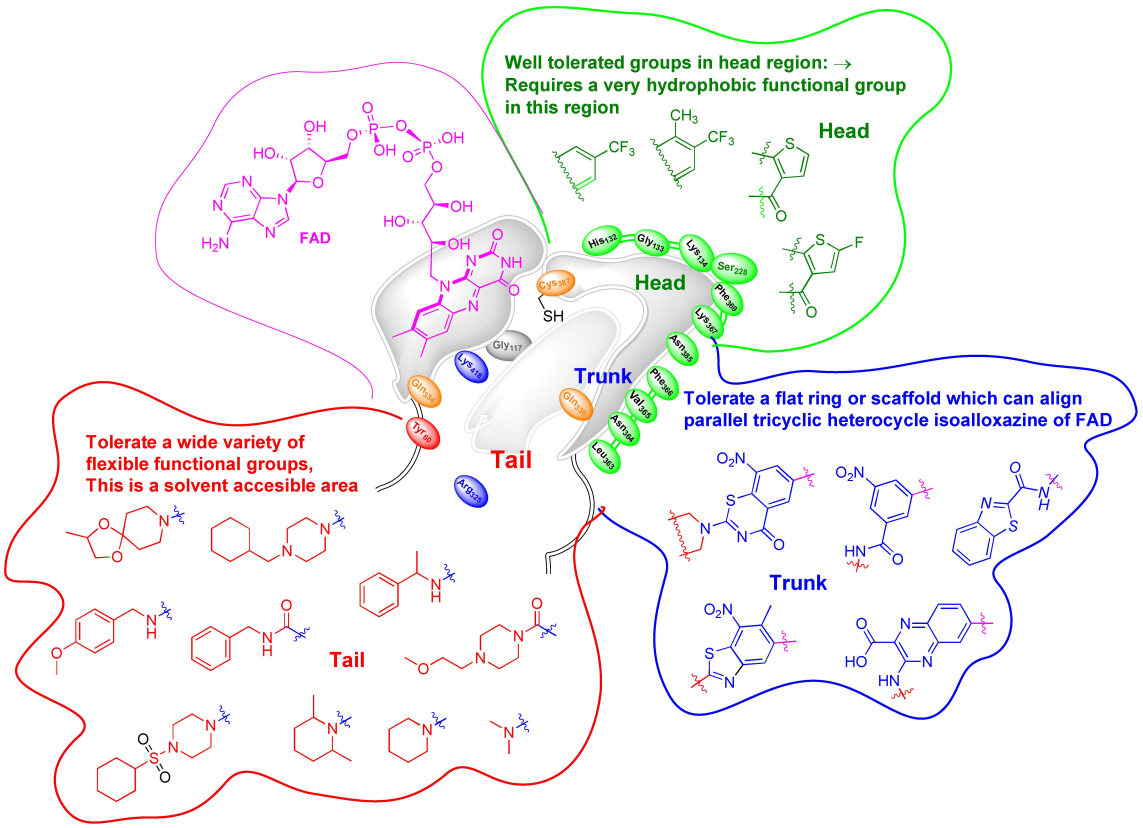

Figure 4. Active site map of DprE1 with important structural landscapes. Tolerable functional groups at different positions in the active site of the DprE1 enzyme are highlighted in green, blue, and red colors respectively for the head, trunk, and tail regions. The color scheme for the binding site is as shown in Figure 3.

The trunk region

This portion runs parallel to the isoalloxazine ring of FAD. The isoalloxazine ring ensures that the substrate and inhibitors remain in a planar orientation within the active site. The trunk is surrounded on one side by the isoalloxazine ring of FAD and Gly117, and on the other side by Gln336, Cys387, Val365, Asn364, and Lys418. Cys387 plays a crucial role in binding covalent inhibitors, forming a covalent bond with nitro groups of compounds such as pBTZ169 (**4**) and BTZ043 (**9**), among others (as seen in Figure 3C).

On the other hand, Lys418 contributes to the stabilization of the covalent adduct by forming an additional hydrogen bond. It forms a hydrogen bond with the carboxamido group of TCA1 (23) (PDB ID 4KW5).[18] and establishes strong hydrogen-bonding interactions with the carboxylate group of the quinoxaline ring (PDB ID 4P8N).[20]

This region is occupied by scaffolds/heterocycles that can align parallel to FAD by forming π-π stacking interactions with the isoalloxazine ring of FAD. The tolerated scaffolds/heterocycles in this region include benzothiazinone, benzothiazole, benzamide, and quinoxaline (see Figure 4). The isoalloxazine ring of FAD forces these rings to fit parallel to it, allowing the ligand to bind to the active site of DprE1. Both monocyclic and bicyclic rings are tolerated in this region. It is important to mention that this region resembles a bulged belly (protruding towards Lys134 and Trp230) and can accommodate slightly larger ring systems, such as tricyclic and macrocyclic planar compounds. The frequently used substructures in this region are shown in (Figure 4). Incorporating flat rings with similar electronic and structural features (i.e. donor/acceptor features) could lead to better DprE1 inhibitors for future use.

The tail region

The last and very flexible region of DprE1 is the tail region. The ligand is generally exposed to the solvent in this region and the flexible loops are poorly resolved in most crystal structures. The tail area consists of two disordered loops; loop I from 269–303 and loop II from 316–330 (Figure 2). Both loops collectively cover the substrate/inhibitor-binding pocket and serve as a gateway for opening and closing the binding site for the substrate or inhibitor.[17] The critical amino acids in this region are Gln334, Tyr60, Leu363, and Arg325. In some crystal structures (PDB ID 4P8N[20]), this region can extend to Asn324, Leu317, Trp230, Asp318, and His315. Tyr60 is a crucial amino acid that forms hydrogen bonds with many co-crystallized ligands. In this region,

various fragments are tolerated, including non-polar aliphatic groups and some aromatic groups. The structural components include piperidine, 2,6-dimethylpiperidine, cyclohexylmethylpiperazine, 4-methoxynenzylamine, and 1,4-dioxa-8-azaspiro[4.5]decane, 4-(cyclohexylsulfonyl)piperidine (Figure 4).

The active site map of DprE1 with important structural landscapes

Tolerable functional groups at different positions in the active site of the DprE1 enzyme are highlighted in green, blue, and red colors respectively for the head, trunk, and tail regions. The color scheme for the binding site is as shown in (Figure 3).

The association of DprE1 and DprE2

The association of DprE1 and DprE2 is crucial for the synthesis of the *Mtb* cell wall and the biosynthesis of the arabinogalactan (AG). The two enzymes form a stable heterodimeric complex, which exhibits better catalytic activity than the individual enzymes.[26] A key finding of the molecular modeling study conducted by the Parkesh group is that DprE1 and DprE2 interact at disordered regions.[26b,27] This interaction may explain the missing electron densities in many crystal structures of the DprE1 enzyme.[28] Thus, it is suggested to consider the structural complex of both DprE1 and DprE2 before conducting any enzyme crystallization or molecular docking experiments on DprE1. In order to ensure accurate and reliable docking results, it is essential to consider structures with complete resolution and no missing residues. Among the available structures, only chain-A in 4P8 L and 4P8T fulfills this criterion. Therefore, for molecular docking studies, focusing on the fully resolved chain-A in 4P8L and 4P8T would provide the most reliable structural information. Additionally, it is important to note that the association between DprE1 and DprE2 can impact ligand binding and efficacy. To obtain more comprehensive results, co-crystallizing a ternary complex consisting of DprE1, the ligand, and DprE2 would be beneficial. This ternary complex structure would yield deeper insights into the ligand binding mode and the interplay between DprE1 and DprE2, potentially leading to improved outcomes in molecular modeling studies.[28] Also developing the DprE2 inhibitors may also help in mutation issue in *Mtb.*

Medicinal Chemistry Perspectives of DprE1 Inhibitors

Several inhibitors of DprE1 have been identified to date, exhibiting either covalent or non-covalent binding to the enzyme. The initial discovery of DprE1 inhibitors involved covalent-binding nitrobezothiazinones (BTZ) analogs, resulting in the clinical candidates BTZ043 (9) and Macozinone (MCZ, PBTZ169, 4).[16–17,24,29] Furthermore, subsequent research has yielded a range of covalent and non-covalent compounds, which will be discussed in the following sections.

The Emergence of Covalent DprE1 Inhibitors

Development of nitrobezothiazinones (BTZs)

Nitrobenzothiazinone represents the earliest and most significant class of covalent DprE1 inhibitors. BTZ043 (9) and BTZ044 (**29**) are the ***S*** and ***R*** enantiomers, respectively, of BTZ038 (**26**) and have equipotent *in vitro* activity (Figure 5A). The ***S*** and ***R*** enantiomers of the amino (BTZ045) and hydroxylamine (BTZ046) derivatives were also synthesized and evaluated, but they showed 500-fold less activity than the nitro analogues.[16] All these compounds form covalent bonds with the Cys387 residue of DprE1. A site-directed mutagenesis study suggests that Cys387 is not essential for DprE1 activity.[30] Hence, for covalent inhibition, a natural substrate such as FAD or its close analogues farnesylphosphoryl-β-D-ribofuranose (FPR) is required for reductive activation of nitro (**26**) to a nitroso intermediate (**27**)[24,31] (Figure 5A). The efficacy of BTZ was determined in the standard mouse infection model, in which BALB/c mice were infected with a bacillary load of *Mtb* H37Rv via aerosol. The pharmacokinetic study of BTZ043 showed a half-life in serum of more than 2 hours, a T_{max} of greater than 0.5 hours, a C_{max} of 2 μg/mL, and an AUC of 4.6 h·μg/mL.

In another experiment by Trefzer *et al.*,[32] it was observed that BTZ043 (**9**) inhibited the epimerization of 14C-DPR into 14C-DPA, confirming that the target enzyme for BTZ043 (**9**) is DprE1. The mutation of Cys394 to Gly394 in $DprE1_{SM}$ (corresponding to Cys387 in $DprE1_{Mtb}$) established resistance against BTZ043 (9) in *Msm* strains. Mass spectrometry studies confirmed the formation of a covalent semi-mercaptal (**28**) intermediate between BTZ043 (**9**) and DprE1SM, demonstrating that BTZs represent a suicide substrate/inhibitor for the DprE1 enzyme.[32] Similarly, Neres *et al.*,[24] established that BTZ043 (**9**) is a pro-drug and that point mutations in DprE1 at Cys387 lead to modulation of MIC values up to 10,000-fold. It was observed that the nitro group of BTZ was essential for anti-TB activity, and these results confirmed that the point mutation at Cys387 was responsible for BTZ resistance.[24,33]

Confirmation of covalent adduct formation

To further support the formation of nitroso-intermediates (**27 and 32**), Liu *et al.*,[34] performed a reduction experiment using BTZ043 (**9**) and PBTZ169 (**4**) and observed the formation of a short-lived intermediate that could be isolated. During the investigation, BTZ043 (**9**) formed a short-lived **Meisenheimer complex** (**30 and 31**), which could be re-oxidized to the original compound (Figure 5B). LC–MS, NMR, and a deute-

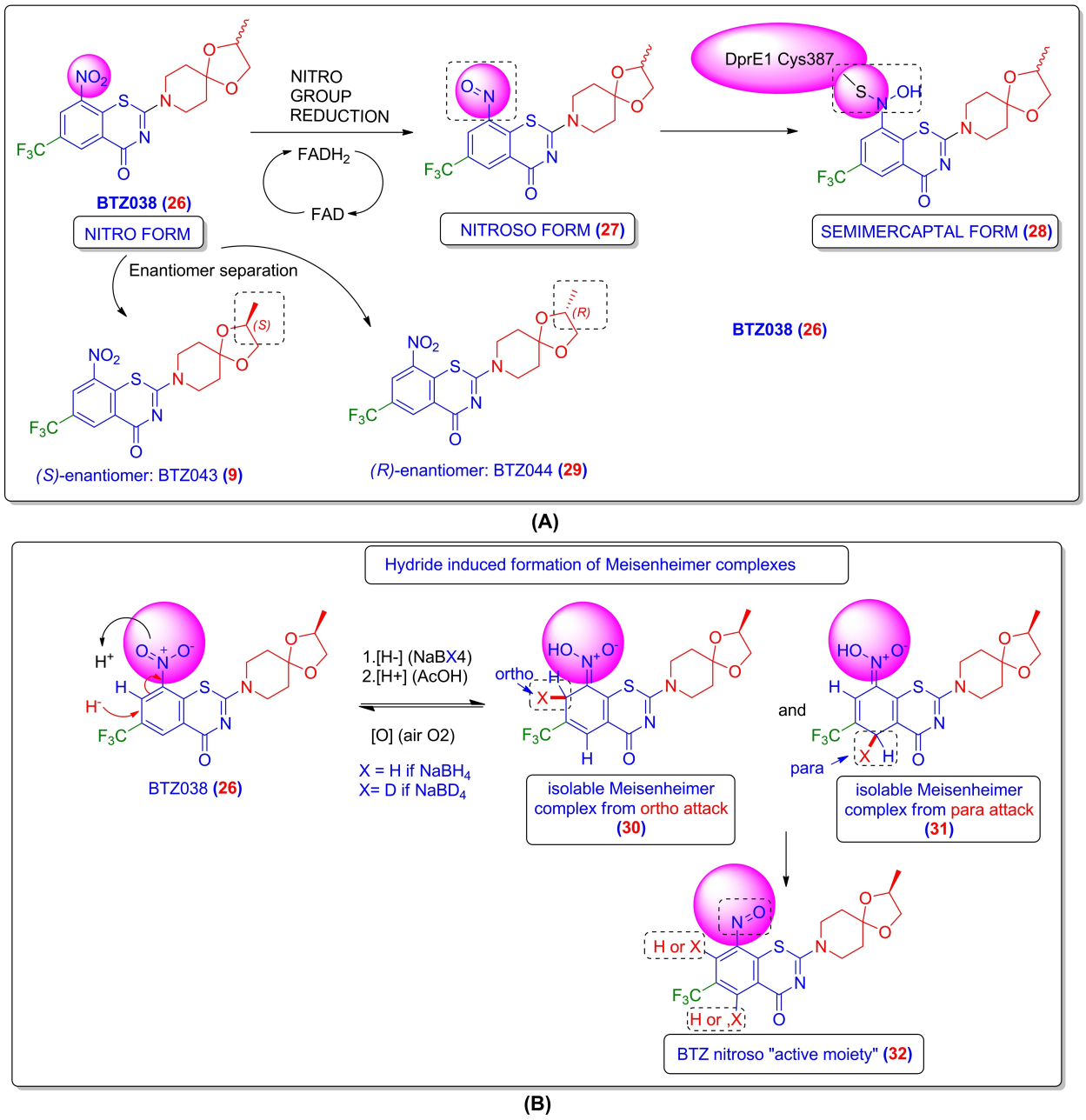

Figure 5. A) Mechanism of semimercaptal adduct formation of BTZ038 (**26**) with Cys387. B) Hydride-induced formation of Meisenheimer complexes. The color scheme is represented according to the binding site (as given in Figure 3).

rium exchange reaction confirmed it, where nucleophile-like hydrides generated using NaBH4 and NaBD4 react directly with BTZ through the addition of ortho (**30**) and para (**31**) to the nitro group. These Meisenheimer complexes appeared differently from BTZ043 (**9**) and PBTZ169 (**4**). When isolated, stored in solution, and exposed to air, they oxidized and regenerated the BTZ nitroso-intermediate (**32**) (Figure 5B).[34]

Proof of subcellular localization of DprE1, its isolation, and first PDB structure elucidation

In their study, Brecik *et al.*[35] utilized high-resolution fluorescence microscopy to identify the extracytoplasmic localization of DprE1, a key enzyme involved in DPA biosynthesis in mycobacteria. The authors provided an explanation for this unexpected finding, highlighting that the periplasmic localization of DprE1 contributes to its vulnerability and the susceptibility of this target to various classes of inhibitors. This extracytoplasmic localization implies that drugs targeting DprE1 can exert their effects without needing to enter

the cytoplasm. As a result, these inhibitors can potentially evade the action of efflux pumps, trapping mechanisms, and other cytoplasmic inactivation mechanisms that might confer intrinsic resistance.

Further, Batt *et al.*,[13e] published two crystal structures of $DprE1_{SM}$ in complex with BTZ043 (**9**) with and without FAD (PDB codes: 4AUT[24] and 4F4Q.[24] As with Batt *et al.*,[13e] some loops were disordered, and electron density maps were missing for the first 13 residues and residues between 275–303 and 330–336. These disordered loops cover the isoalloxazine ring of FAD, which is located at the interface between the substrate/inhibitor-binding and cofactor-binding domains. They found that Lys425 (corresponding to Lys418 in *Mtb*) is a crucial amino acid for DprE1 activity, which was confirmed through site-directed mutagenesis experiments. A mutation of Lys425 to Ala425 resulted in complete loss of DprE1 activity. The group also synthesized a fluorescent-labeled BTZ043 (**9**) analogue known as **BTZ-TAMRA** (**33**), which had moderate activity (6.2 μg/mL MIC_{99}) against *Mtb* H37Rv and localized to DprE1 (Figure 6A). The localization of DprE1 within the bacterial cell was investigated, and fluorescence analysis revealed distinct localization at the poles of the bacteria, suggesting the subcellular localization of DprE1 for the first time. The crystal structure of the native and BTZ043-bound DprE1 showed that the active site required a conformational change to accommodate the DPR substrate. Two disordered loops were observed between residues 323–329 and 275–303 (Figure 6B and 6C).[13e,36]

Discovery of macozinone (MCZ), a piperazine-containing benzothiazinone (PBTZ)

To optimize the potency and toxicity of BTZ043 (**9**), Makarov *et al.*,[19] discovered the clinical candidate PBTZ169 (**4**), or Macozinone (MCZ). The evaluation of BTZ043 (**9**) in a mouse model revealed that it had a weak potency and high hydrophobicity, and therefore, the authors proposed to alter its molecular structure in order to enhance its drug profile and improve its efficacy. Instead of the piperidine scaffold, they incorporated a piperazine ring in a new series of benzothiazinones (BTZs) and obtained PBTZs as improved DprE1 inhibitors. Extensive SAR studies were performed by substituting the N-4 piperazine. Hydrophilic groups, such as carboxylic acids, alcohols, and different amines, resulted in reduced anti-TB activity compared to BTZ043 (**9**). Aromatic hydrophobic substituents, such as a phenyl ring, were not tolerated. Aliphatic alkyl substitutions at N-4 were attempted, resulting in improved water solubility and better potency due to protonation of the tertiary amino nitrogen of the piperazine ring. *In vitro* activities against *Mtb*H37Rv showed a strong correlation between minimum inhibitory concentra-

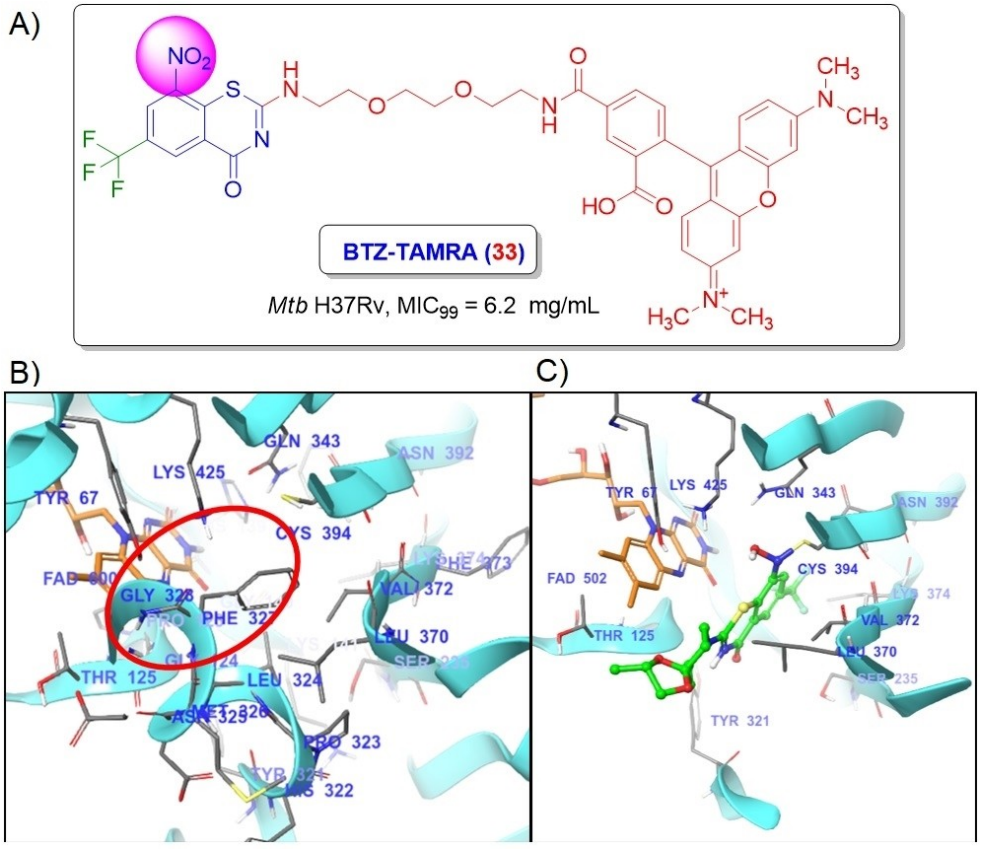

Figure 6. A) 2D structure of BTZ-TAMRA (**33**). **B**) Crystal structure of 4AUT,[24] an apo form. **C**) Crystal structure of 4F4Q co-crystallized with BTZ043 (**9**).

tion (MIC) and lipophilicity. **PBTZ169** (**4**) was found to be twenty times more potent than BTZ043 (9) (MIC_{99} *Mtb* H37Rv = 0.003 μg/mL) and possess better stability in the mouse model. *In vivo* efficacy of PBTZ169 in a murine model of chronic TB after low-dose aerosol infection of BALB/c mice was assessed and found to be active in both lungs and spleen and superior to BTZ043 in reducing bacterial burden in the spleen and CFU in the lungs by more than 0.5 log, equivalent to isoniazid. Compared to BTZ043, pharmacokinetic data suggest that PBTZ169 is rapidly absorbed in the stomach and intestine and has a serum level that remains well above the MIC for more than 21 hours with a single daily dose. PBTZ169 (**4**) (TD_{50} = 58 μg/mL) was found to be less toxic than BTZ043 (**9**) (TD_{50} = 5 μg/mL) in the HepG2 human cell line. A crystal structure of *Mtb* DprE1 covalently bound to PBTZ169 (**4**) was obtained with a resolution of 1.9 Å (PDB 4NCR.[19] Nearmedic Plus LLC is conducting a Phase 2a clinical study for PBTZ169 (**4**), although its current status is "terminated (very slow enrollment).[29e]"

Binding mode analysis of PBTZ169 (4)

The binding mode of PBTZ169 (4) to DprE1 has been studied by Makarov *et al.*,[19] and found to be similar to that of BTZ043 (**9**). PBTZ169 (4) binds to the substrate/inhibitor-binding pocket with its -NO_2 group covalently binding to Cys387 and the -CF_3 group situated in a hydrophobic pocket. The BTZ ring is aligned parallel to FAD, and the piperazine ring and cyclohexyl form Van der Waals interactions with Gly117, Trp230, and Leu363. The cyclohexyl-methyl moiety lacks electron density and is exposed to the solvent (Figure 7B).

Optimization efforts on BTZ043 (9) and PBTZ169 (4)

Optimization of BTZ nucleus led to the development of N-alkyl and heterocyclic ring-substituted 1,3-benzothiazine-4-one derivatives. In this series, compound **34** (Figure 7A) displayed a minimum inhibitory concentration (MIC) of 0.0001 μM against *Mtb* H37Rv, 20 times higher activity than BTZ043 (**9**). The pharmacokinetic properties of compound 34 were determined in Sprague Dawley rats through single oral (p.o.) and intravenous administration (i.v.). The elimination half-life was found to be approximately 2.5 hours (i.v.) and 5.4 hours (p.o.), and C_{max} was achieved through oral dosing at about 0.56 μg/mL (1.25 μM), which is 12,560 times higher than its *in vitro* MIC level. It also showed an acceptable oral bioavailability of 26%. The increase in activity might be due to the replacement of the spiroketal group with an azaspirodithiolane group.[37] On the other hand, Li *et al.*[38] identified a benzothiopyranone analogue (**35**) (Figure 7A) through scaffold morphing of BTZ as a DprE1 inhibitor. SAR studies revealed that benzothiopyranone analogues with a tertiary amino side chain at the 2-position showed potent activity. In this study, compound (**35**) displayed excellent *in vitro* activity against *Mtb* H37Rv and two XDR-TB clinical isolates, and superior pharmacokinetic properties in male Balb/c mice, with high plasma exposure and a prolonged elimination half-life of approximately 7.25 hours after oral administration, and low oral bioavailability of 13.1%. *In vivo* efficacy was evaluated in a murine model of acute infection with *Mtb* H37Rv, resulting in a 5.4 log reduction of *Mtb* colony-forming units (CFU) in the lungs.[38]

Tiwari *et al.*,[39] discovered two oxidation products of BTZ043 (9), benzothiazinone-sulfoxide (BTZ-SO) (**36**) and benzothiazinone-sulfone (BTZ-SO2) (**37**). The metabolic fate of BTZ043 (9) was governed by either a cytochrome P450 or a flavin monooxygenase enzyme. The compounds were evaluated against pathogenic mycobacterial strains, such as *Mtb* and *Mycobacterium bovis*, and BTZ-SO (**36**) was found to be effective and showed impressive activity, while BTZ-SO2 (**37**) showed mild activity (as seen in Figure 7A).[39]

Piton *et al.*,[22] revised the SAR of PBTZ and discovered the novel series of sulfonyl benzothiazinones (sPBTZ) through structural modification at the piperazine-N-4 position. This modification improved the metabolic stability, *in vivo* activity, and aqueous solubility of the compounds. Among these, sPBTZ11626091 (**38**) (as seen in Figure 7A) was found to be the best. The SAR studies showed that substitutions with small groups (methyl, ethyl, cyclopropyl) on the sulfonyl moiety led to mild cytotoxicity, higher solubility, and better metabolic stability due to low clearance rates. Substitutions with larger functional groups were more toxic, less soluble, and had high clearance rates and less metabolic stability. The *in vivo* efficacy of sPBTZ11626091 was evaluated in a murine model of chronic TB and was found to reduce the bacterial burden in lungs and spleen by 0.46 ($P < 0.05$) and 1.03 ($P < 0.0001$) $\log_{10}$, respectively. The results were validated by solving the crystal structures of DprE1 in complex with sPBTZ169 (**14**) with a resolution of 2.40 Å (PDB 6G83[22]) and the interactions were similar to those of pBTZ169 (Table 1).

More efforts to improve PBTZ169 (**4**) were undertaken by Zhang *et al.*.[40] They synthesized unique spirocyclic and bicyclic-8-nitrobenzothiazinones that showed improved physicochemical and pharmacokinetic properties when compared to the reference. The best compound (**39**) (Figure 7A) had a minimum inhibitory concentration (MIC) of 32 nM (0.014 μg/mL) and showed a 1000-fold improvement in solubility. It also had a 2-fold lower clearance rate compared to PBTZ169 (**4**). The compound showed oral bioavailability of 27% and a high volume of distribution, resulting in a terminal elimination half-life of 2.5 hours. SAR studies revealed that compounds that retained piperazine-like properties showed better inhibition activity. The study showed that high lipophilicity and molecular symmetry increased potency, while reducing molecular planarity improved solubility.

Gao *et al.*,[41] identified benzothiazinethiones as a new scaffold as anti-TB agents, which were obtained by thiolation of benzothiazinones. One of the potent benzothiazinethione analogs, SKLB-TB1001 (**40**), is shown in the box in (Figure 7A) and demonstrated excellent activity against *Mtb*. The inhib-

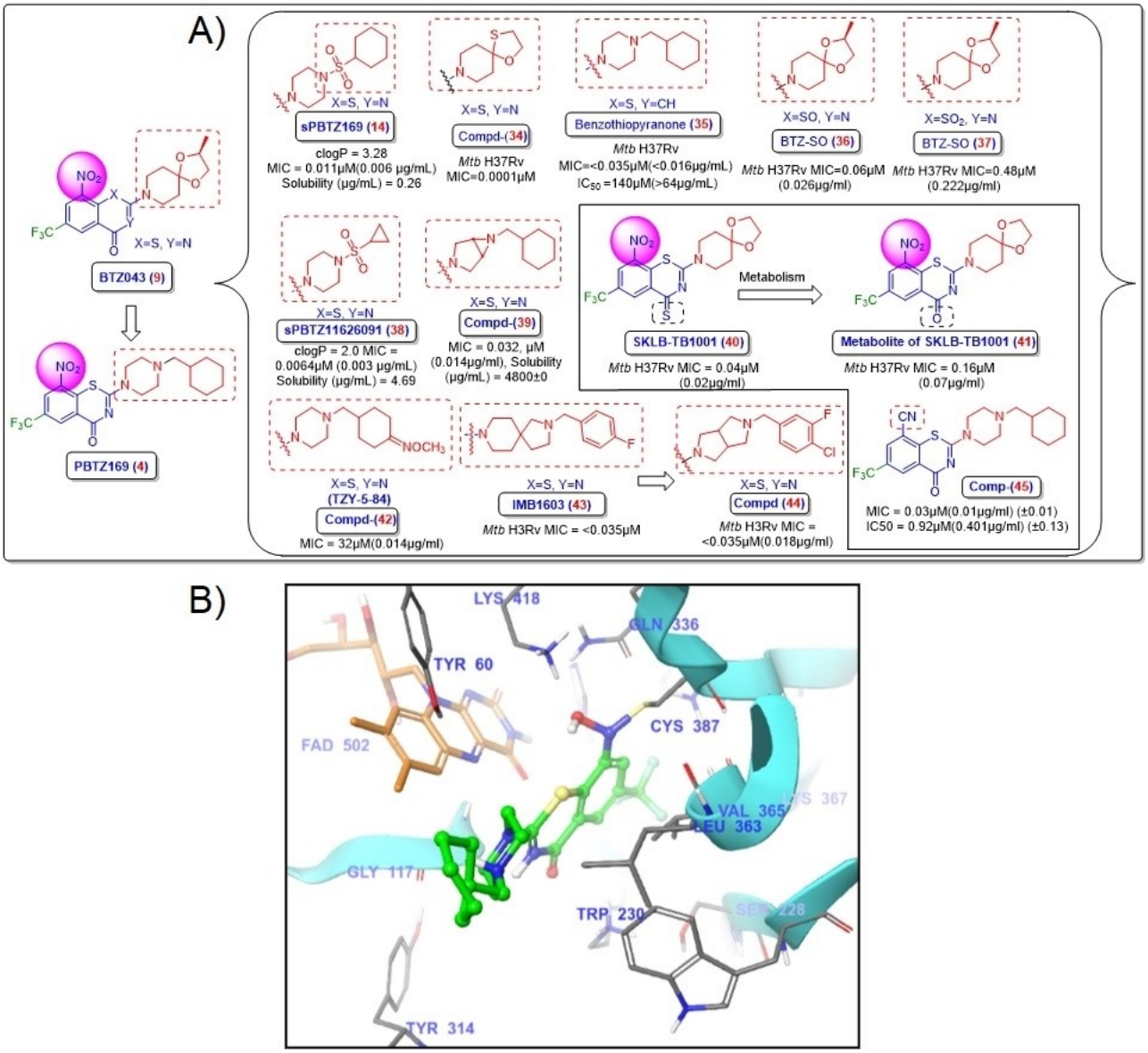

Figure 7. Discovery of macozinone and others (**14**-**45**). **A**) Rationale for the discovery of novel BTZ and other derivatives. **B**) Binding mode of **PBTZ169** (**4**) with DprE1 (PDB 4NCR[19]).

ition of DprE1 by SKLB-TB1001 (40) was confirmed through computational docking and differential scanning calorimetry. It is speculated that SKLB-TB1001 (**40**) may have a unique mechanism of action as it may generate a sulfur-containing metabolite or an organic SO_2 donor, which could bind to DNA or RNA due to the nucleophilicity of the S atom. The compound was found to be as potent as BTZ043 (**9**) and PBTZ169 (**4**) against replicating H37Rv and was more potent than isoniazid (MIC-0.064 μM/0.47 μg/mL). It was similarly potent against multidrug-resistant clinical strains that showed resistance to isoniazid and rifampicin, and it was equipotent against extensively drug-resistant clinical strains. SKLB-TB showed favorable oral bioavailability in lipophilic formulation, suggesting a high potential for clinical trials at higher doses. A pharmacokinetic profile study was conducted in SD rats at a dose of 5 mg/kg, and the results showed rapid absorption with a T_{max} of 1.13 hours and a moderate elimination half-life of 1.45 hours.[41] In an *in vivo* metabolic identification experiment of SKLB-TB1001 (**40**), seven metabolites were isolated, but only the de-sulfuration oxidation metabolite (**41**) showed moderate activity against H37Rv.[42]

Wang *et al.*,[43] developed a series of potent benzothiazinones containing an oxime moiety (**42**) (Figure 7A) attached to a nitrogen heterocycle through the cyclohexyl ring of PBTZ. 19 compounds were screened, and among them, one was close to PBTZ and showed greater potency than PBTZ. This compound is under evaluation as a potent anti-TB clinical candidate. *In vivo* efficacy was performed on a murine model infected with *Mtb* H37Rv strains and compound (**42**) was found to reduce CFUs in the lungs by 4.04 logs, which is

greater than PBTZ169 but less than isoniazid. Pharmacokinetic profiles were conducted in SD rats at a single intravenous dose (2.5 mg/kg) and oral multi-dose at 20, 50, 200 mg/kg, which showed T1/2 of 1.77 ± 0.43, 3.20 ± 0.71, 4.13 ± 1.27, and 6.73 ± 1.41 respectively, which is greater than PBTZ169[43] The compound (**42**) was renamed **TZY-5-84** and further studied by Guo *et al.*.[44] It showed potent *in vitro* activity against *Mtb* H37Rv, ranging from 0.014 to 0.015 mg/L. In the murine infection model, at a dose of 12.5 mg/kg, it showed comparable efficacy to PBTZ169 at a dose of 25 mg/kg.[44]

More recently, Lu and colleagues identified and optimized a series of novel spiro-heterocycles through the hybridization of PBTZ169 (**4**) and BTZ043 (**9**). The best compound from this series, IMB1603 (**43**)[45] (Figure 7A), was found to have a similar activity profile and better solubility compared to PBTZ169 (**4**). The IMB1603 (**43**) was found to have a MIC value of < 0.035 μM against *Mtb* H37Rv. Further research was carried out by Ma *et al.*,[46] and they identified hexahydropyrrolo[3,4-*c*]pyrrole clubbed benzothiazones as potent compound. The activity of these agents was optimized by making changes at the 2-position of BTZ. SAR findings suggested that substituents on the phenyl ring play a crucial role in *Mtb* activity, with para and meta substituents showing comparable potency to ortho-substituted BTZs, and double substituents (para and meta) showing even better potency than mono-substituted BTZs. For instance, a compound with 4-chloro-3-fluorophenyl substituent (**44**) showed excellent activity against *Mtb* (MIC < 0.035 μM/0.018 μg/mL) with low cytotoxicity and better water solubility compared to PBTZ169 (**4**)[46]

Liu *et al.*[47] investigated covalent inhibitors, which have stronger and longer-lasting interactions with target proteins compared to non-covalent inhibitors, leading to better pharmacological responses at lower concentrations. They replaced the nitro-electrophile of BTZs with other warheads, and studied three classes of BTZ derivatives (Figure 7A). Only compound **45** (cyano group replacing nitro-group of PBTZ169) showed moderate potency with a MIC of 0.03 μM and IC_{50} of 0.92 μM. However, none of the compounds showed covalent DprE1 inhibition[47]

Efforts to replace BTZ core ring

Development of dinitrobenzamide derivatives (DNBs) and more

In search of new DprE1 inhibitors, Christophe *et al.*,[33] conducted a high-throughput phenotypic screen using automated confocal microscopy, which led to the identification of dinitrobenzamide derivatives (DNBs) with excellent activity against drug-sensitive, MDR, and XDR strains of *Mtb*. SAR studies indicated that the nitro group at the 3 and 5 positions on the benzene ring is most favored, and reducing one of these nitro groups to an amine or hydroxylamine group resulted in reduced activity. **DNB1** (**46**) (Figure 8) showed excellent biological activity in both extracellular (MIC 0.2 μM) and intracellular (MIC 0.2 μM) assays. The cyclic benzamide derivative **47**-(***S***) was more potent in extracellular assays (MIC 0.08 μM) but less potent in intracellular assays. These DNBs showed time-dependent bactericidal action and had a good ADME profile[33]

Xanthone derivatives-methyl-2,4,7-trinitroxanthone (MTX)

Based on the discovery of BTZs and DNBs, Trefzer *et al.*,[30b] discovered two classes of compounds: 1) methyl-2,4,7-trinitroxanthone (**MTX**, xanthone derivatives) and 2) dinitrobenzene derivatives (**DNBs**). MTX (**48**) (Figure 8) was found to have anti-TB activity against both BTZ-resistant and BTZ-sensitive strains, with a mechanism of inhibition and resistance similar to other BTZs. SAR studies showed that only one of the nitro groups in MTX was essential for its biological activity. Further optimization led to the discovery of CT319 (**13**) (Table 1), which had high activity against both *Msm* and *Mtb* and contained a -CF3 group in place of one of the nitro groups. Both CT319 (**13**) and MTX (**48**) have a -NO2 warhead and a similar resistance mechanism. It was also observed that the nitroso-intermediate forms the semi-mercaptal adduct instead of the nitro-group, confirmed by synthesizing nitroso-derivative CT325 (**12**) fromCT319 (**13**).[30b] The crystal structure of DprE1MT with CT325 (**12**) was determined and the atomic coordinates of five crystal structures were deposited in the Protein Data Bank (PDB) server (e.g., 4FDN, 4FDO, 4FEH, 4FDP, and 4FF6)[13e] (**See** Table 1 for PDB details and their ligands).

Based on the discovery of BTZs, Tiwari *et al.*[48] developed a series of anti-TB compounds. The activity of BTZ derivatives depends on an electron-deficient nitro-aromatic core and the 2-methyl-1,4-dioxa-8-azaspiro[4.5]decane can be replaced with various functional groups. The BTZ scaffold was simplified to simpler nitro-aromatic compounds, and the linker-groups were varied through sulfonamide (**49**), benzyl esters (**50**), and reverse-amides (**51**). SAR studies showed that di-nitro substitutions were the best and less electrophilic compared to CF_3 substitutions or unsubstituted compounds, especially in sulfonamide(**49**).[48]

Discovery of benzothiazole N-oxides (BTO)

Landge *et al.*,[20,49] discovered a nitro-arenesbenzothiazole (**BT**) series using a whole cell-based phenotypic screening campaign, with a benzothiazole-oxide (**BTO**) emerging as a promising scaffold. The exploration of benzothiazole chemistry led to the discovery of different compounds, namely BTO, BT, and crowded benzothiazoles (**cBT**). A comparison of all series in terms of IC_{50} values revealed that potency decreases in the following hierarchy: BTO < BT < CBT. The best compound in the BTO series was (**10**) (Table 1) with an MIC of 0.05 μM (0.02 μg/mL) against *Mtb* H37Rv and an inhibitory activity IC_{50} of 0.026 μM (0.011 μg/mL) against *Mtb* DprE1. The compounds from the BT series were moderately

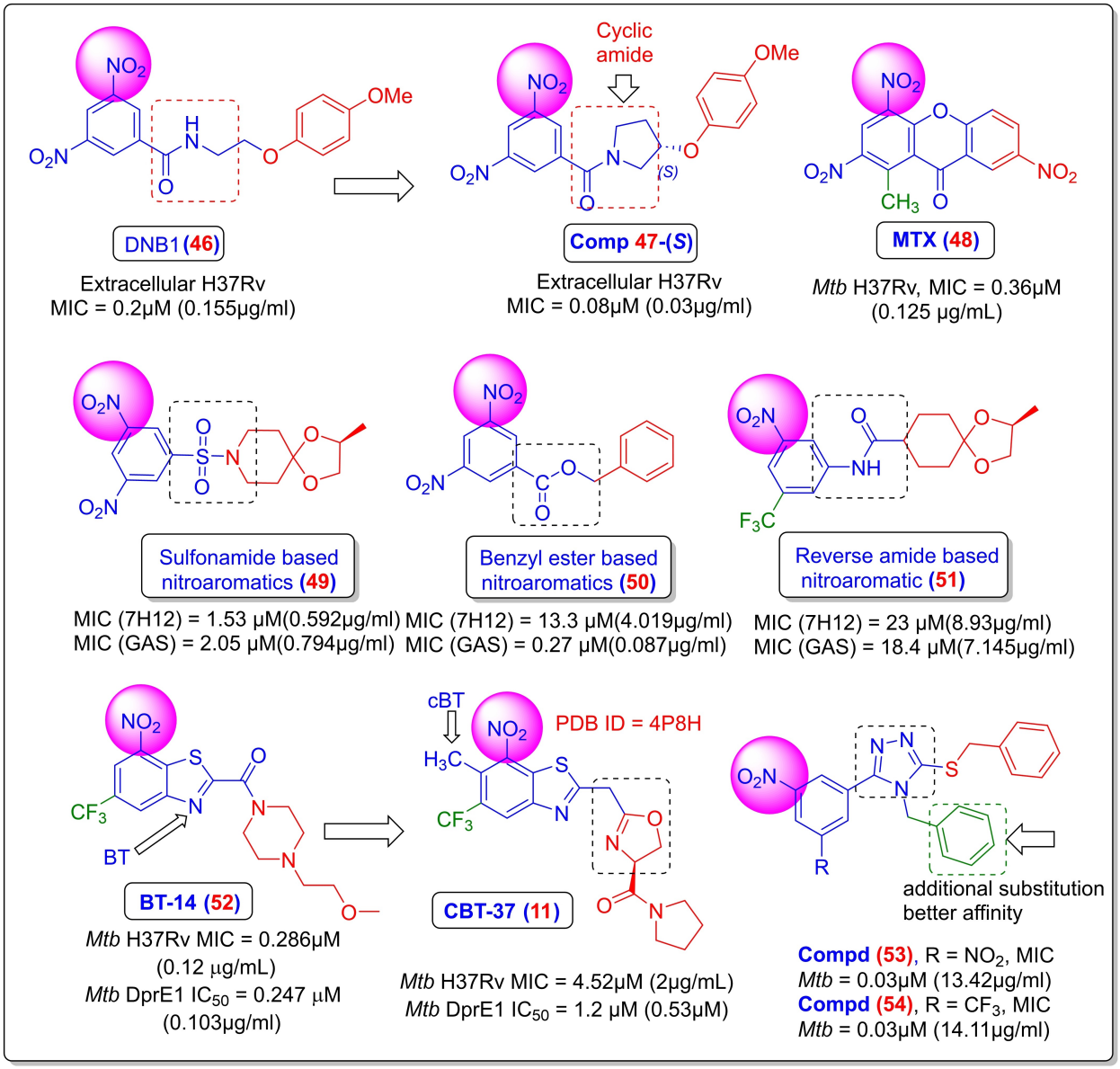

Figure 8. Discovery, SAR, and optimization of DNBs, BTs, and CBTs (**46**-**54**).

active, with the best compound (BT-14, **52**) (Figure 8) having an activity MIC of 0.286 μM (0.12 mg/mL) against *Mtb* H37Rv and an IC_{50} of 0.247 μM (0.103 μg/mL), but were found to be mutagenic. The cBTs were found to possess reduced potency, which may be due to the steric hindrance caused by the methyl group around the nitro group. As a result, the nitro-group in cBTs may not be reduced into a nitroso-group, which occurs in the normal activation of benzothiazoles. However, the reduced potency was advantageous as cBTs are the safest, most stable, least cytotoxic, and non-mutagenic. To assess the importance of the nitro group, replacements with a nitrile, sydnone group, or boronic acids were tried at this position, but these replacements resulted in inactive compounds against *Mtb*. To assess the importance of the CF_3 group at position-5, a nitrile group was incorporated, but the resulting compound was less potent than the original BT. However, when an amide group replaced the CF_3 group, the resulting compound was inactive, possibly due to its inability to form a covalent bond. When an amide group was introduced at position-2, the resulting compounds CBT-18 (**19**) (Table 1) showed an increase in MIC values: *Mtb* H37Rv MIC = 4.6 μM (2 μg/mL), *Mtb* DprE1 IC_{50} = 1.7 μM (0.735 μM). The replacement of the amide with an oxazoline ring resulted in the discovery of the novel compound CBT-37(**11**) with almost a similar potency profile: *Mtb* H37Rv MIC = 4.52 μM (2 μg/mL), *Mtb* DprE1 IC_{50} = 1.2 μM (0.53 μM).

Finally, to understand the binding mode of these series of compounds, CBT-18 (**19**) and CBT-37 (**11**) were co-crystallized with DprE1**TB**. Interestingly, it was observed that despite having the same nucleus as methyl CBT-18 in 4PFA, CBT-18

binds covalently while CBT-37 in 4P8H binds non-covalently. The methyl group located adjacent to the -NO2 group in the CBTs was necessary for its balancing effect; it decreases electron affinity and nullifies the mutagenic effect of the nitro group, thus offering a better safety profile[49] (Figure 8). In general, BTO and BT compounds were found to be cytotoxic, mutagenic, and exhibit CYP inhibition, while CBT-containing compounds did not. This observation may be due to the hindrance effect of the methyl group on these reactions.

Discovery of 1,2,4-triazole analogues

Roh and colleagues[50] discovered many anti-tuberculosis (TB) compounds containing the nuclei of oxadiazole, triazole, and tetrazole.[50–51] The mechanism of action of these compounds was found to be similar to that of PBTZ169 (4). Based on the patented oxadiazole-containing compounds, a series of 1,2,4-triazole analogues (isosteres of 1,3,4-oxadiazole) was prepared and demonstrated excellent anti-mycobacterial activity. Compounds (53) and (54) were found to be effective against MDR/XDR strains of *Mtb* at an MIC of 0.03 μM = 13.42 μg/mL (Compound (53), = 14.11 μg/mL Compound (54) (Figure 8). Roh and colleagues found that m-dinitrobenzene and m-CF_3-NO_2-benzene as substituents were equally potent in their study[50–51]

Development of Noncovalent DprE1 Inhibitors

Covalent DprE1 inhibitors have proven to be successful as anti-TB agents and have produced many clinical candidates. However, they may induce mutagenicity and cross-reactivity issues with off-target enzymes. Therefore, non-covalent DprE1 inhibitors have the potential to meet the requirements for bioactivity while minimizing the negative effects associated with covalent DprE1 inhibitors. The subsequent section details the evolution of various classes of non-covalent compounds.

Discovery of benzothiazole based non-covalent DprE1 inhibitors

Wang and colleagues discovered the few pioneering non-covalent benzothiazole-based DprE1 inhibitors.[18] Cell-based phenotypic screening identified TCA1 (**23**) (Figure 9 and Table 1) as the first non-covalent DprE1 inhibitor against *Mtb* MDR and XDR strains. The MIC against WT *Msm* was found to be 0.23 ± 0.012 μM, while against the mutant (Y314 C) *Msm*, it was 5.4 ± 0.32 μM. Similarly, the IC_{50} against *Msm* DprE1WT was 0.048 ± 0.014 μM, while against the mutant (Y321 C) *Msm* DprE1, it was 0.24 ± 0.052 μM. TCA1 (**23**) was found to possess bactericidal activity against both replicating and non-replicating *Mtb*. The crystal structure of $DprE1_{TB}$ in complex with TCA1 (PDB-4KW5[18]) was released with a resolution of 2.61 Å (Figure 15A). The active site analysis of DprE1 revealed that TCA1 (**23**) has many interaction points in the active site, resulting in excellent potency[18] (the detailed explanation is given in the Ligand Interaction Analysis section). In the animal model study, TCA1 upon i.v. administration showed a low clearance, a steady-state volume of distribution, and an elimination half-life of 0.73 h. After oral administration of a 20 mg/kg or 50 mg/kg solution formulation, it exhibited a high C_{max}, moderate exposure with a bioavailability of 19% to 46%, respectively, and a half-life of 1.8 h. It was also stable to proteolytic activity in human and mouse plasma for up to 4 h and had no inhibitory activity against four CYP enzymes. *In vivo* efficacy experiments were performed on acute and chronic infection models using a 100 mg/kg dose. After four weeks of administration of TCA1, the CFU dropped nearly 2 logs in the lungs and more than 3 logs in the spleen in the acute model. In the chronic infection model, TCA1 showed efficacy in both the lungs and the spleen, with a CFU reduction of 1 log and 1.4 logs, respectively. After identifying TCA1 (**23**), Liu *et al.*,[21] discovered several new derivatives of TCA1 with improved *in vitro* potency, *in vivo* efficacy, and better pharmacokinetic properties. The incorporation of the nitrogen group into the benzothiazole ring led to the formation of TCA481 (**24**) and TCA007 (**55**) (Figure 9). Due to their better activity and pharmacokinetic properties, TCA007 (55) was selected for further biological evaluation in an aerosol-infected BALB/c mouse model. After three weeks of administration of TCA007 (50 mg/kg and 100 mg/kg), a dose-dependent reduction in the CFU was observed, with 1.7 and 2.3 logs, respectively. However, benzothiazoles were found to irreversibly interact with CYP4502C9, a major cytochrome P450 enzyme, which may cause drug-drug interactions and present serious issues in combinatorial drug regimens.[21]

Discovery of azaindole and benzimidazole (BI) based non-covalent DprE1 inhibitors

Following the discovery of TCA1 and its analogues, Shirude *et al.*,[52] used scaffold morphing to discover different 1,4-azaindole and benzimidazole (BI) derivatives. They took the imidazopyridine nucleus as a reference scaffold. The authors started with the imidazopyridine (**56**) scaffold (Figure 9) and identified the azaindole ring as the best core to fit into the active site of DprE1. The reported ligand had low bactericidal potency, so they used scaffold morphing to improve its activity. They replaced the imidazopyridine scaffold with the 1,4-azaindole core, resulting in better bactericidal activity. Incorporating a 6-methyl group in the 1,4-azaindole (**57**, also known as **TBA-7371**) core improved cellular potency (MIC 0.78 μM/0.277 μg/mL) compared to the unsubstituted ring. SAR analysis showed that the amide group is essential for activity, and amide side chains containing small hydrophobic groups (e.g., cyclopropyl-methyl, fluoro-ethyl, and hydroxyethyl) are well tolerated in the active site. These substitutions also influenced the physicochemical properties and

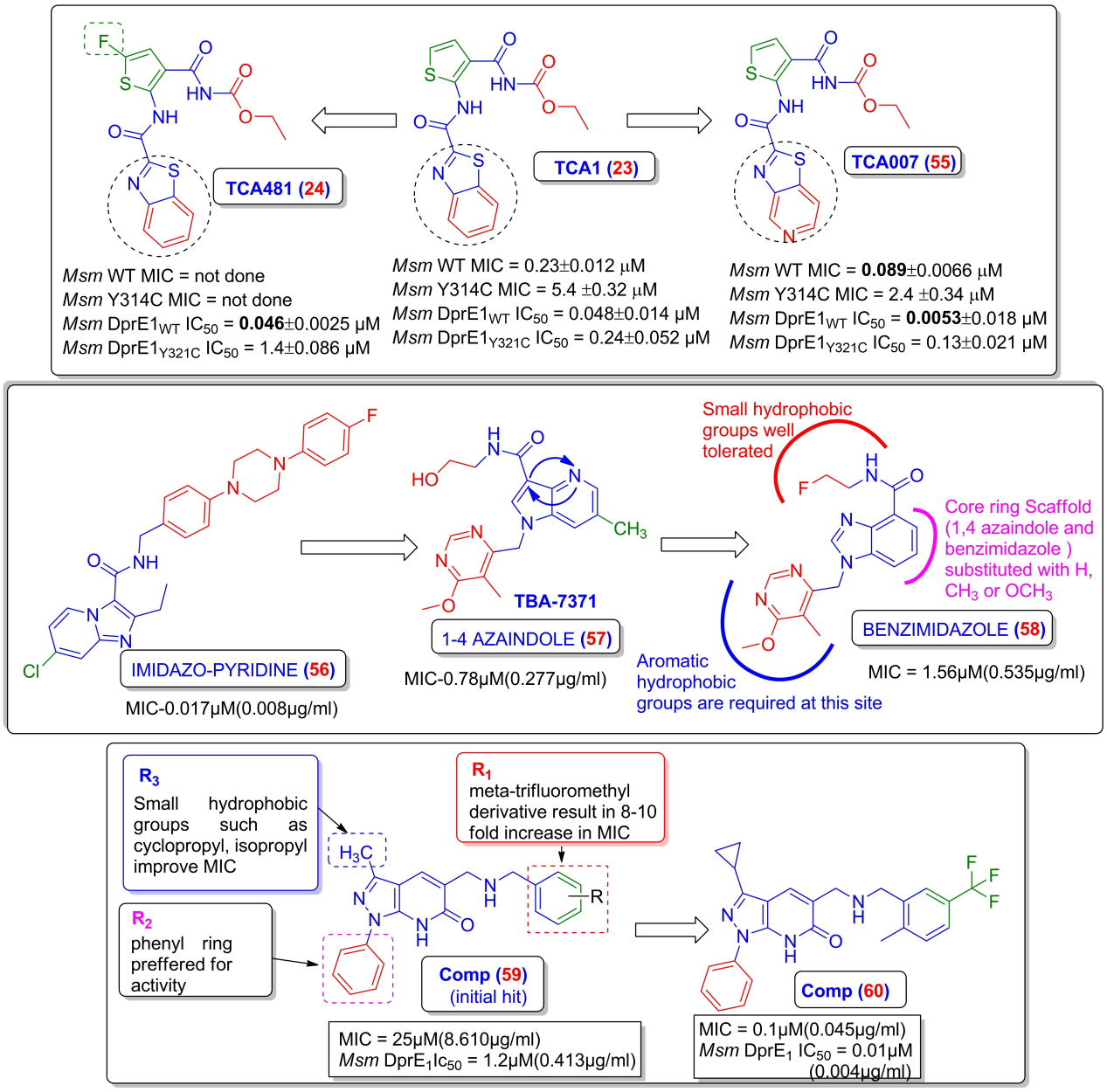

Figure 9. Development and optimization of benzthiazole, azaindole, benzimidazole, and pyrazolopyridone-based non-covalent DprE1 inhibitors (**55**-**60**).

in vitro safety parameters. The authors reported that the N–H of the amide group might be involved in intramolecular hydrogen bonding with the nitrogen (N4) of the azaindole ring or with DprE1.[52] The amide side chain also influenced physicochemical properties such as solubility and *in vitro* safety parameters. The hydroxyethyl amide side-chain substitution increased mouse liver microsome (MLM) stability compared to the hydrophobic amide side chain.[52]

In another study, the same core substituted with benzyl group can tolerate various di-substituted benzyl and di-substituted heteroaryl-methyl groups, which weakly inhibit the host enzyme PDE6 and result in poor visual activity. *In vitro* PDE6 SAR studies found that 6-methoxy-5-methylpyrimidine-4-yl still retained hydrophobic interactions, and the amide side chain continued to maintain meaningful hydrogen bond donor-acceptor interactions with DprE1. However, replacement of this group with 6-(dimethylamino)-5-methylpyrimidine-4-yl resulted in reduced PDE6 inhibition.[53] Both benzimidazole (**58**) and 1,4-azaindole (**57**) were found to be active against *Mtb*, and based on comprehensive pharmacokinetic studies, azaindoles (**57**) have good bioavailability and a moderate clearance rate, making them suitable for further clinical evaluation.[52,54] The Bill and Melinda Gates Medical Research Institute is currently conducting a phase 2a dose escalation, controlled, randomized study to evaluate the safety, early bactericidal activity,

and pharmacokinetics of **TBA-7371** in adult patients with rifampicin-sensitive pulmonary tuberculosis.[55]

Pyrazolopyridones based non-covalent DprE1 inhibitors

Through a whole-cell screening method, Panda and colleagues[56] discovered a new class of pyrazolopyridones. The lead compound (**59**) (Figure 9) consists of an N-aryl pyrazolopyridone ring with a basic amino linker attached to a phenyl ring, with a modest MIC of 25 μM (8.610 μg/mL) against *Mtb*. SAR studies revealed mainly three diversification points, R1, R2, and R3. Initially, the R3 position was optimized to a methyl substitution as phenyl or larger groups were detrimental for biological activity. Then, it was observed that the substitution of methyl with a cyclopropyl group resulted in MIC improvement. The phenyl group at R1 was then optimized, and it was found that the *meta*-CF_3 group, instead of an unsubstituted phenyl ring, led to an 8-fold increase in MIC. Replacement of *meta*-CF_3 group with a nitrile group leads to decreased activity. This suggests the importance of CF_3 in binding to the active site. Finally, the R3 was fixed as an unsubstituted phenyl group, as the substituted rings were unfavorable for activity. Further SAR studies revealed that substitution of the –NH linker with an amide group resulted in diminished potency. After the optimization of this series, Compound (**60**) (Figure 9) was found to be the most potent, with an IC_{50} of 0.01 μM (0.004 μg/mL) and MIC of 0.1 μM (0.045 μg/mL). The DMPK properties studies found that the most potent compound had a log D value of 3.5, while the solubility, free plasma protein binding, and clearance were optimum. The rat liver hepatocytes clearance was found to be high, and human microsomal clearance was decent. The safety margin of the pyrazolopyridone series was accessed by testing the compounds against the human A549 cell line, and it was found that the selectivity index (SI) for compound 63 was >250.[56]

Development of aminoquinolone (AQs)-linked piperidineamides as non-covalent DprE1 inhibitors: Naik *et al.*,[57] identified a novel 4-aminoquinoline piperidine amide scaffold compound (**56**) via whole-cell-based screens as a non-covalent reversible DprE1 inhibitor. They confirmed that AQs bind to DprE1 in a non-covalent reversible manner using mass spectrometry and enzyme kinetics analysis. SAR of AQs was divided into three parts, as given below (Figure 10).[57]

Site 1

The aminoquinolone ring at site-1 is crucial for the activity as its replacement with other bicyclic rings resulted in weakly active compounds. Introducing a fluorine atom at C-6, C-7, and C-8 improved potency as seen with Compound (**62**), which had a MIC of 0.8 μM (0.337 μg/mL) against *Mtb*. Alkyl substitution on N-1 is detrimental to activity due to the loss of H-bonding with the Asn385 in the active site (Figure 10).

The linker

When N–H at C-4 was replaced with O or NCH_3, very weak activity was observed. The substitution of the piperidine ring with an alicyclic ring at the linker position resulted in a more ineffective compound. In contrast, improved MIC was shown in substituted pyridines and bicyclic systems having a piperidine core (Figure 10).

Site-2, the aryl ring

Di-substituted five-membered heterocyclic rings such as pyrazole, isoxazole, and triazoles were well tolerated. The substitution at C-5 of the pyrazole ring was found to be crucial for potent DprE1 inhibitor activity. A chloro or methyl substitution at this position improved the activity, which may be due to favorable hydrophobic interactions in this site. However, substitution with any group larger than ethyl on N-1 of the pyrazole ring was found to be detrimental for inhibitory activity.

Although attempts to co-crystallize AQs with DprE1 have been unsuccessful, the information gained from structure-guided design has led to the development of very potent compounds, such as Compound (**63**), which possesses a MIC of 0.06 μM (0.025μg/mL) and an IC_{50} of 0.007 μM (0.002μg/mL).[57] *In vitro* bactericidal activity of aminoquinolones showed a maximum kill of 4 log by day 14. Compounds containing di-fluoro substitution at the 6 and 7 positions of the quinolone ring exhibited a kill of 3 log by day 3 and 4 log by day 7. These compounds were also found to be effective against non-replicating phase *Mtb* and drug-resistant strains of *Mtb*, but were found to be inactive against all non-mycobacterial strains. The hypoxia model of NRP *Mtb* was used for the non-replicating phase and found that all the compounds were inactive, suggesting that DprE1 is responsible for cell wall synthesis. When the compounds were tested against all single-drug resistant strains, results indicated that the compounds could potentially treat drug-resistant tuberculosis. All amino-quinolones were tested for pharmacokinetics and *in vitro* DMPK properties, such as solubility, logD, human plasma protein binding, and human microsomal clearance. The solubility of all the compounds was low, ranging from 6 to 100 μM, but it was improved from 3 to 5-fold in FeSSIF media (fed-state simulated intestinal fluid). *In vitro* plasma protein binding of NH quinolone analogues showed a greater unbound fraction in human plasma, and free NH-quinolones possessed poor Caco-2 permeability and a high efflux ratio. The cytochrome P450 isoforms were not inhibited by any of the quinolone compounds tested. In general, unsubstituted piperidine ring compounds exhibited hERG $IC_{50}>33$ M, although some compounds with the bicyclo[3,2,1]octanyl ring, like **63**, had hERG $IC_{50}<33$ M. This may be due to the higher logD of these compounds (see Figure 10).

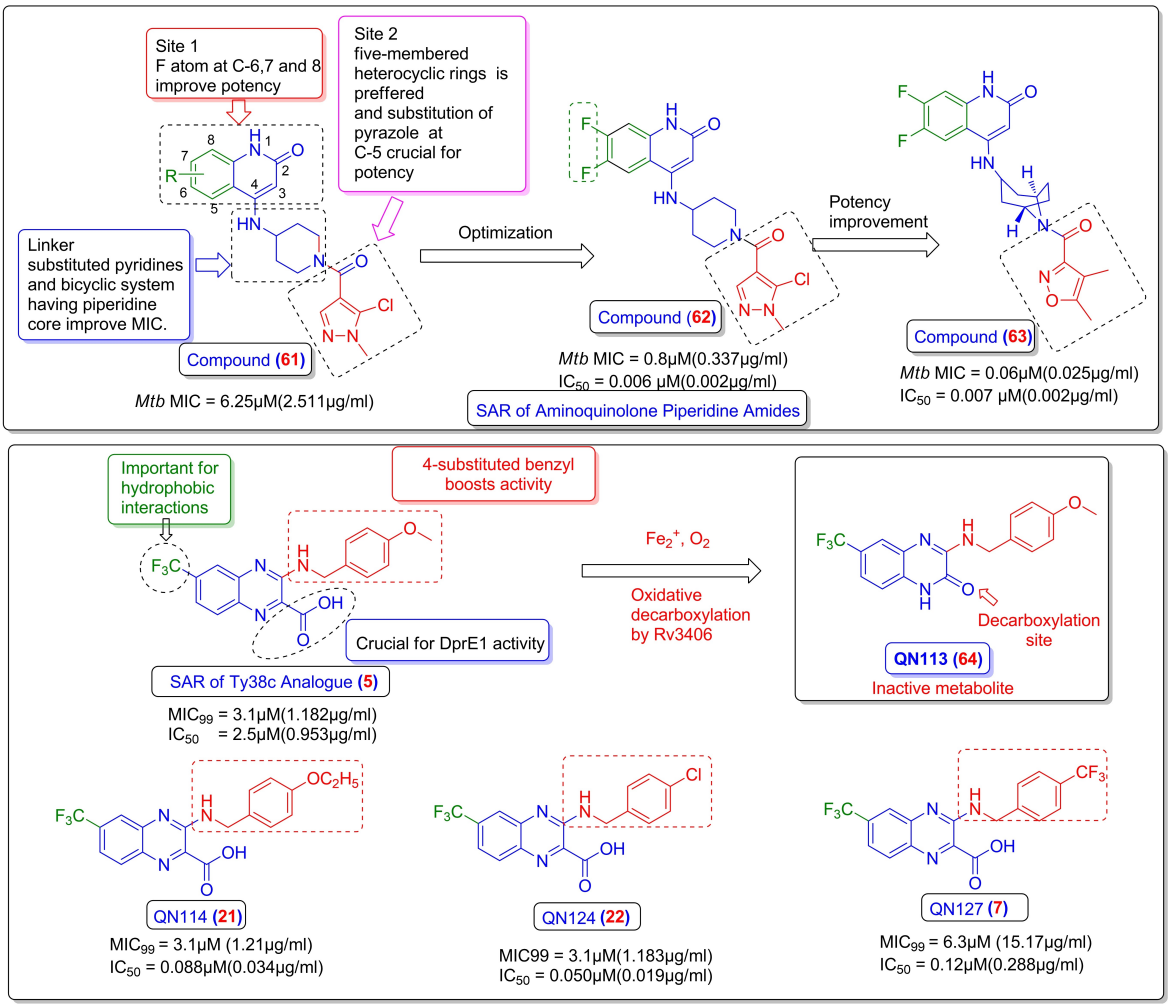

Figure 10. Development and SAR of AQ-piperidineamides and aminoquinolonepiperidine-amides and 2-carboxyquinoxalines as non-covalent DprE1 inhibitors (**61**-**64**).

Discovery and development of 2-carboxyquinoxalines-based non-covalent DprE1 inhibitors

In their study, Neres *et al.*,[58] discovered a new class of quinoxaline-based non-covalent DprE1 inhibitors with anti-TB activity. The lead compound Ty38C (**5**) (Figure 10) was found to be active against both intracellular and extracellular *Mtb*, with an IC_{50} of 2.5 μM (0.953 μg/mL). Further SAR studies aimed to improve the potency of this compound and address its inactivation by the Rv3406 gene, which encodes an α-ketoglutarate-dependent sulfate ester dioxygenase that converts Ty38C (**5**) to an inactive compound QN113 (**64**) (Figure 10) via oxidative decarboxylation.

SAR analysis showed that substituting the 2-carboxylate group with methyl, carboxamide groups keto analogues or resulted in inactive compounds. While the 2-carboxy ethyl esters exhibited reasonable MIC values. At position 3 of the quinoxaline ring, the benzyl group was found to be preferred over phenyl groups, enhancing interaction with the active site. A para-substitution on the benzyl group generated potent compounds, such as Ty38C (**5**), QN114 (**21**), QN124 (**22**), and QN127 (**7**), all of which had MIC_{99} values of 3.1 μM and IC_{50} values of 0.041, 0.088, 0.050, and 0.12 μM, respectively. However, a meta-substitution on the benzyl group led to a loss of potency. Finally, the researchers co-crystallized Ty38C (5) and several other analogues with DprE1 TB (e.g., 4P8C, 4P8K, 4P8L, 4P8N, 4P8P, 4P8T, and 4P8Y).[58] However, no further studies on these molecules have been published.

Hydantoin-based DprE1 inhibitors

Target-based high-throughput screening efforts discovered unique hydantoin derivatives that are unrelated to other DprE1 inhibitors. Compound (**65**) (Figure 11) was the best amongst the series with a pIC_{50} of 7.0 and an MIC of 8.3 μM (3.065 μg/mL). It also possessed admissible lipophilicity and good solubility with no cytotoxicity. Upon careful analysis, it was found that the hit compound contains four different pharmacophoric features: **ring A, ring B, linker**, and **the core**

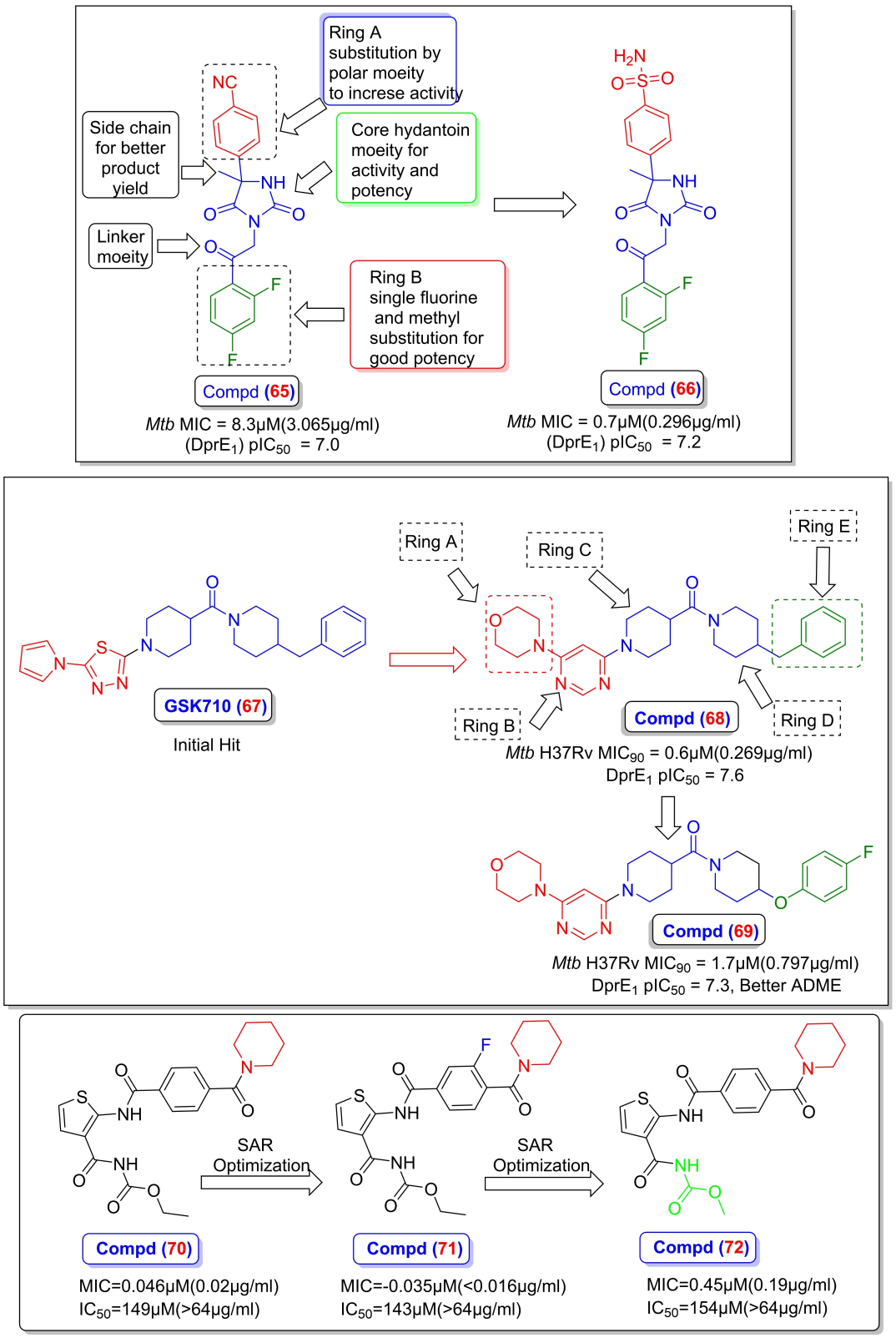

Figure 11. Discovery and development and SAR of hydantoin, pyrrolothiadiazole, and thiophenearylamide based non-covalent DprE1 inhibitors (**65**-**72**).

ring of the hydantoin moiety. The hydantoin core ring and acetyl moiety are essential for biological activity. Polar substitution on ring A, e.g., a cyano group, leads to a molecule with a similar inhibitory response with no cytotox-

icity. Substitution of polar groups on **ring A** improves activity, of which primary sulfonamides gave excellent MIC improvement. Initially, the racemate of compound (**65**) was prepared and tested for activity. Subsequently, isolation and testing of both isomers were done, and it was found that the (*R*)-enantiomer was more potent than the (*S*)-enantiomer in an enzymatic assay (pIC_{50} 7.2 and 4.2, respectively) as well as in whole-cell assays (MIC 6.7 μM and >125 μM, respectively). Substitution with methyl sulfonamide on **ring A** retained activity, whereas nitrogen sulfonamide did not. The introduction of the methyl group on the hydantoin ring did not affect the activity of the compound. However, linker modulation, keto group removal, or methylation resulted in decreased potency. Further modifications made to the hydantoin ring did not produce any significant changes, indicating that the hydantoin core is crucial for interacting with DprE1. It was also recommended that N1-nitrogen was important for enzyme binding. In terms of **ring B**, various modifications were prepared. The lead compound, 2,4-difluorophenyl ring, was found to be the most potent of all the derivatives. Substituting the groups like cyclohexyl, thiophene, and naphthalene on **ring B** preserved potency. Concluding optimization led to the development of compound (**66**) (Figure 11), which possesses an excellent MIC of 0.7 μM (0.296 μg/mL) and a good pIC_{50} of 7.2. *In vitro* metabolic stability was examined for the compound (**66**), and it was found to possess excellent metabolic strength with 0.4 ml/min/g in the human microsome and ADMET profile. *In vivo* therapeutic efficacy of compound **66** was determined in a C57BL/6 J mouse model. After oral administration, the results showed a 0.5 log reduction in CFU units. This demonstrates that the compound (**66**) has a limited *in vivo* efficacy compared to the reference compound moxifloxacin. The compound also showed a C_{max} value of 6380 ng/mL and AUC of 31400 h·ng/mL. It was also revealed that these series work via a reversible inhibition mechanism[59,60]

Pyrrolothiadiazole-based DprE1 inhibitors

Through phenotypic screening, Borthwick *et al.*,[31,61] identified a new class of pyrrolothiadiazole DprE1 inhibitors with reduced activity in a DprE1 overexpressor strain of *Mtb*. The lead optimization of the initial hit (**GSK710, 67**) was done through sub-structure and similarity search to develop a novel series of potent analogues. This search resulted in the development of a potent compound (**68**) with an MIC_{90} of 0.6 μM (0.269 μg/mL) against *Mtb* H37Rv and a DprE1 pIC_{50} of 7.6. SAR studies on compound (**68**) (Figure 11) revealed that small branched and alicyclic amines substituted on **ring A** resulted in less active compounds than the parent piperidine. Specifically, a benzyl group was highly potent and achieved a sub-micromolar MIC against *Mtb*. Initial removal of either **ring A** and **B** or **AB** and **E** resulted in no activity, while other analogues showed weak activity. Similar activity to the pyrimidine with good ligand efficiency was demonstrated with the oxidized core. The substitution of the piperidine linker (**Ring C**) and **Ring D** showed no further improvement in activity. The pyrrolidine analogue showed similar potency. Substituting the benzylic group in **Ring E** with a heteroatom led to improved intrinsic clearance. Substituting the phenyl ring with a pyridine retained activity, but alkyl group resulted in the loss of activity. Compound **69**, which was discovered by replacing the benzylic group of compound **68** with substituted phenoxy groups, exhibited excellent potency and low MIC values ($MIC_{90}=1.7$ μM or 0.797 μg/mL). Overall, the compounds obtained through property-focused optimization showed good potency, low MIC, and improved DMPK properties. The *in vivo* efficacy study was conducted in an acute model of TB infection, and the results demonstrated that compounds **68** and **69** were highly effective with an ED_{99} value of 30 mg/kg.[61]

Thiophene arylamide based non-covalent DprE1 inhibitors

Inspired from TCA1, Wang *et al.*,[62] identified a series of thiophene-arylamide compounds with increased activity and druggability through scaffold hopping. The molecular modeling studies revealed that acyl piperidine might increase binding affinity and thus boost antimycobacterial activity. Through SAR analysis, it was found that benzamides, e.g., compound (**70**) (Figure 11) (MIC-0.046 μM/0.02 μg/mL), showed better antimycobacterial activity. Next, the effect of the aryl moiety was explored with the introduction of halo, nitro, and methyl substituents on the phenyl moiety that can form π-π interactions in the hydrophobic pocket of the active site. Substitution with fluoro, chloro, and bromo groups afforded compounds with good activity, among which the compound bearing the electron-withdrawing fluoro group (**71**) (MIC-0.035 μM/<0.016 μg/mL) at the phenyl ring was best tolerated at the aryl site and showed a 10-fold enhancement of potency. In the end, substitution at the carbamate was explored. Compared to TCAI, compounds with imide methyl ester, such as compound (**72**), showed better antimycobacterial activity with the MIC of 0.19 μg/mL. These potent compounds were next subjected to testing against XDR-TB strains. Compounds (**70**) and (**71**) in comparison to TCA1 (**23**) showed very potent efficacy against both drug-susceptible and drug-resistant tuberculosis *in vitro*. An additional experiment was also performed to determine the MIC of the representative drugs against PBTZ169 (**4**) and bedaquiline-resistant M. tuberculosis strains. The cross-resistance study done for PBTZ169 (4) and bedaquiline indicated that all the compounds tested are non-covalent DprE1 inhibitors. The compounds (**70**) and (**71**), had improved intracellular activity with a reduction of 1 log_{10} CFU (compared to TCA1 $=0.61$ log_{10} CFU). These compounds were subjected to *in vitro* ADMET assay and none of them exhibited cytotoxicity in HepG2 cells while showed low inhibition of the hERG channels. Following a single oral and intravenous dose, pharmacokinetic (PK) investigations for compounds (**71**), (**72**), and TCA1 (**23**) were carried out in Balb/c mice. After oral treatment, compound (**72**) had high

plasma exposure (AUC_0-∞ = 657 ng·h/mL) and maximum plasma concentration (C_{max} = 486 ng/mL), compared to compound (**71**), which had AUC_0-∞ = 57.9 ng·h/mL and C_{max} = 25.4 ng/mL. TCA1 (**23**) had 5-fold better oral bioavailability than (**72**). In an acute TB infection model, the *in vivo* efficacy of compound (**72**) was tested in Balb/c mice. Compound (**72**) showed strong *in vivo* activity, reducing the bacterial burden in the lungs by 2.02 $\log_{10}$ CFU after the oral administration of a 100 mg/kg dose. Compared to TCA1 (**23**), these results demonstrated that compound (**72**) had similar efficacy even at reduced bioavailability.[62]

Carbostyril-based DprE1 inhibitors

Hariguchi *et al.*,[63] screened a library of carbostyril analogues and optimized a 3,4-dihydrocarbostyril derivative and identified OPC-167832 (**73**)[64] (Figure 12) as a very potent *Mtb* bactericidal agent. It has a low MIC range of 0.00024–0.002 μg/mL for *Mtb* H37Rv and is active against different types of drug-susceptible strains, MDR, and XDR strains. This compound has similar bactericidal activity to rifampicin (MIC-0.30 μM/0.25 μg/mL), moxifloxacin (MIC-1.24 μM/0.5 μg/mL), and levofloxacin (MIC-1.38 μM/0.5 μg/mL) against *Mtb*. As OPC-167832 (**73**) does not contain any reactive warhead and binds non-covalently with DprE1, the possibility of getting resistance against *Mtb* is lower than with BTZ043, even with a mutation at Cys387.[56] The OPC-167832 (**73**) works on *Mtb* in two different ways: one is through Rv0678 (non-targeted) gene mutation, which is a repressor for the MmpS5-MmpL5 efflux pump, and the other is through Rv-3790 (targeted) gene mutation as a DprE1 inhibitor. With any anti-TB agent, OPC-167832 (**73**) does not show an antagonistic effect. After single and combinational *in vitro* studies, it was found that it showed higher efficacy with delamanid and bedaquiline and showed no effect with linezolid. The PK profile of OPC167832 (**73**) was examined at different doses in normal ICR female mice. After oral administration, the peak plasma concentration was found to be 0.5–1 h, and the elimination half-life was 1.3–2.1 h. The distribution of OPC-167832 (**73**) in lungs was two times higher than that in plasma. Overall, OPC-167832 (**73**) has potential therapeutic activity with a good pharmacokinetic and safety profile. Therefore, in combination with other anti-TB agents, this drug can be used for *in vivo* experiments.[63] The Otsuka Pharmaceutical is conducting clinical studies (Phase 1/2) on OPC167832 (**73**).[65] Looking at the promising results of OPC-167832, in August 2021, the Bill & Melinda Gates Foundation granted $17.8 million in research funds to Otsuka Pharmaceutical for further clinical trials in phase IIb.[66] OPC-167832 (**73**) is the first candidate among DprE1 inhibitors that has entered Phase IIb.

Other Noncovalent DprE1 Inhibitors

N-Alkyl-5-hydroxypyrimidinone carboxamide-based DprE1 inhibitors

Oh *et al.*,[67] screened a library of 6207 compounds containing pyrimidinedione for inhibitory properties. Only compound (**74**) (Figure 13) was found to be active in replicating conditions (*Mtb* MIC = 4.7 μM (1.961μg/mL). Compound (**74**) is an N-methyl-5-hydroxypyrimidinedione with substituted benzyl and benzyl-substituted carboxamides on each side. The SAR studies showed that the presence of a benzene ring on the left-hand side of the compound's structure was crucial for *Mtb* activity. Furthermore, the potency of the compound was improved when the benzene ring had an -ortho-CF_3 substituent. On the other hand, when the benzene ring was absent, the compound lost all activity. The modification on the right-hand side of the scaffold revealed the significance of the benzyl amide group for the compound's activity. The activity decreased when the benzyl group was substituted with phenyl. Compound (**74**) possesses acceptable cytotoxicity and pharmacokinetic properties, including toxicity. Pharmacokinetic properties of compound (**74**) performed on C57BL/6 mice administered a single 10 mg/kg were found to be pretty low: C_{max} 0.25 μg/mL, a half-life of 4 h, and a volume of distribution of 33.7 L/kg. *In vitro* bactericidal activity of compound (**74**) was observed to reduce 1–2 logs in CFU after seven days with a weak dose-dependent effect.[67]

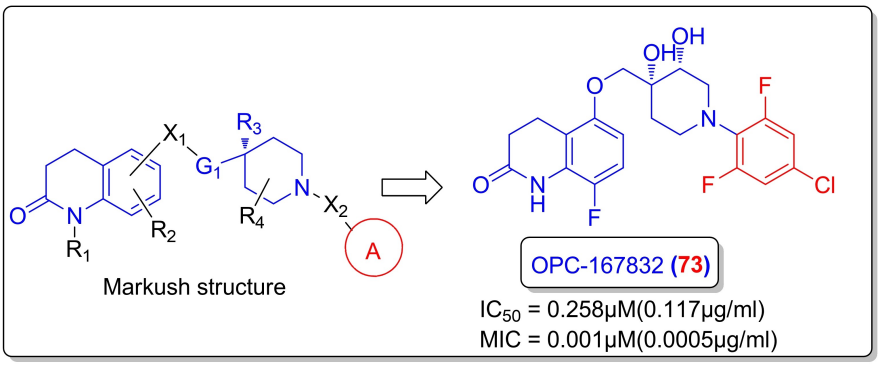

Figure 12. Structure and development of OPC167832 (**73**).

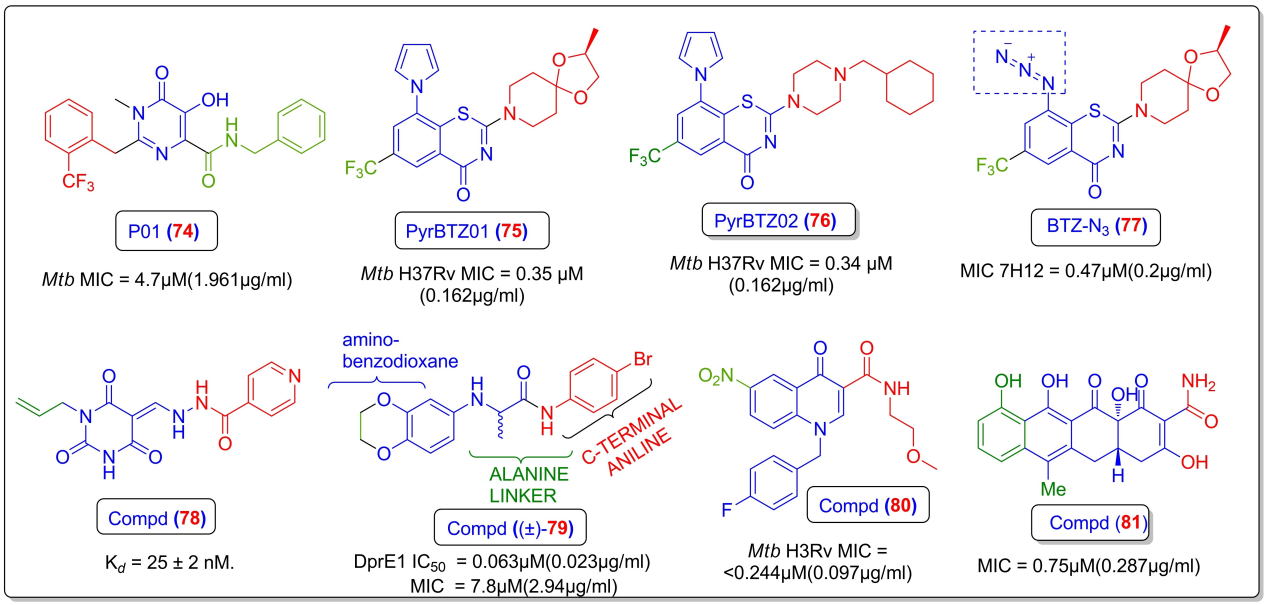

Figure 13. Structures of some other potent non-covalent DprE1 inhibitors (**75**-**81**).

8-Pyrrole-benzothiazinones based DprE1 inhibitors

8-Pyrrole-benzothiazinone-based DprE1 inhibitors were synthesized by Makarov *et al.*,[68] namely PyrBTZ01 (**75**) (Figure 13) and PyrBTZ02 (**76**), which are pyrrole-based analogues of BTZ043 (**9**) and PBTZ169 (**4**), respectively. The only difference between the existing and new derivatives is the replacement of the 8-NO_2 group with an 8-pyrrole ring, and both compounds showed moderate anti-mycobacterial properties (MIC *Mtb* H37Rv = 0.35 μM (0.162 μg/mL) and 0.34 μM (0.162 μg/mL), respectively). PyrBTZ01 (**75**) and PyrBTZ02 (**76**), the two most potent analogues, were characterized to determine their mode of action. Both compounds showed activities against BTZ-resistant strains with a 600-fold increase in MIC and were confirmed to target DprE1. The docking studies of PyrBTZ analogues with PDB 4NCR[19] revealed that the active site of DprE1 can accommodate both compounds by placing the pyrrole ring in the vicinity of Cys387 and maintaining the overall binding mode of the BTZ ring system. The pyrrole ring is placed below Cys387 and leads to the minor embedding of PyrBTZ analogues. The induced-fit docking results revealed that a conformational change in either Lys418 or Trp230 stabilizes the pyrrole compound in the pocket. Cytotoxicity studies were also performed against four human cell lines, and the results showed that both compounds were less toxic, with PyrBTZ02 (**76**) found to be least harmful than BTZ043 (**9**). Both compounds were not found to be mutagenic when tested in SOS Chromotest. Intrinsic clearance, i.e., in-vitro metabolic stability, was evaluated using mouse and human liver microsomes, and both compounds showed intermediate clearance values similar to BTZ043 (**9**) and PBTZ169 (**4**). Next, an *in vivo* pharmacokinetic study of PyrBTZ01 (**75**) in BALB/c mice was performed in comparison with BTZ043 (**9**). The results showed that the dose of 25 mg/kg of both compounds had similar half-lives of 100 minutes. However, when an *in vivo* efficacy study was performed using a mouse model of acute TB for PyrBTZ01 (**75**), the result showed that PyrBTZ01 (**75**) was not effective against the mouse model of acute TB.[68]

1,3-Benzothiazinone azide (BTS-N_3)-based DprE1 inhibitors

Tiwari *et al.*,[69] discovered a very different analogue of benzothiazinone after the discovery of 8-pyrrole benzothiazinones by replacing the nitro group with the electron-withdrawing azide group. Although the BTZ-N_3 (**77**) showed excellent activity (MIC 7H12 = 0.47 μM (0.2 μg/mL)) it was poorer than BTZ043 (**9**) (Figure 13). Computational docking studies suggested that it binds in the same pocket as that of BTZ043 (**9**). Biochemical studies with the cell envelope fraction of *Msm* in combination with biochemical studies indicated that the azide analogue has a different activation mode than BTZ043 (**9**). BTZ043 (**9**)is a covalent inhibitor of DprE1 while, BTZ-N_3 is a reversible and non-covalent DprE1 inhibitor.[69]

Pyrimidinetrione based DprE1 inhibitor

Gao *et al.*,[70] used virtual screening to sort approximately 6.2 million compounds from the ZINC and natural product databases against DprE1 (PDB 4FDO).[70–71] After screening, total 63 compounds were selected. *In vitro* inhibition tests using *Mtb* and *Msm* indicated that one compound among the 63 compounds was bactericidal. The compound (**78**) (shown in Figure 13) was active against acute TB infection with a Kd value of 25 ± 2 nM, which is comparable to isoniazid. To test

the *in vivo* bactericidal activity of compound (**78**), the authors used an acute infection mouse model. After administering the compound at 10 and 30 mg/kg and the reference drug INH at 10 mg/kg, the CFU count reduced to 1.0 log in the lungs and 0.6 log in the spleen for compound (78) (10 mg/kg), which was similar to INH. Moreover, the CFU count reduced to 2.1 log in the lungs and 1.3 log in the spleen for compound (78) (50 mg/kg).[70] A cytotoxicity study was performed for compound (78) to assess its safety *in vitro* and *in vivo*, and no cytotoxicity was observed.

Phenylpropanamide based DprE1 inhibitors

Whitehurst *et al.*,[72] discovered a new scaffold, 2-((2,3-dihydrobenzo[b][1,4]dioxin-6-yl)amino)-N-phenylpropanamides, as a potent non-covalent DprE1 inhibitor. The initial hit (**79**) (shown in Figure 13) was found to have potent DprE1 inhibitory activity with an IC_{50} of 0.063 μM (0.023 μg/mL) or a pIC_{50} of 7.2. This compound was reported to have good *Mtb* activity in a whole-cell assay (*Mtb* MIC of 7.8 μM/2.94 μg/mL). Further SAR studies led to the development of multiple analogues that possessed potent DprE1 inhibitory properties. From the study of physicochemical properties, compound (**79**) was found to possess a high lipophilic value (Chrom $LogD_{7.4} = 5.5$). A pharmacophore analysis revealed that the structure contains three main features: an amino-benzodioxane, an alanine linker, and a C-terminal aniline. The issue of lipophilicity was addressed by removing the substitution at the α-position of the alanine linker. The addition of a lactam resulted in a compound with no activity, while nitrogen analogues and tetrahydronaphthalene were found to be less potent than dioxane. Para-substitution in the aniline with a lipophilic character, such as para-Cl and para-CF_3, showed more potency with greater DprE1 inhibitory activity. However, para-substitution with a polar character, such as para-nitrile, showed moderate potency and moderate MIC values. A fused bicyclic ring compound retained DprE1 inhibitory activity, but less than the original hit.[72]

Nitroquinolone-based DprE1 inhibitors

In a recent study, Dube *et al.*,[73] discovered a series of 6-nitroquinolone-3-carboxamide derivatives as DprE1 inhibitors. Quinolones and nitro-containing compounds were found to exhibit good pharmacokinetic properties. Different combinations were prepared by substituting the N-1 and R-3 positions of the quinolone ring. Among the 23 compounds evaluated for *Mtb* activity, 12 compounds showed activity ranging between < 0.244 μM and 31.865 μM, with the most potent agent being compound (**80**) (Figure 13) with a MIC of < 0.244 μM (0.097 μg/mL). SAR studies indicate that substituting aliphatic side chains at the C-3 position is well-tolerated, rather than cyclic chains. The N-1 part of quinolone accepts 4-substituted benzyl groups rather than 3-substituted benzyl groups. Molecular docking studies of compound (**80**) revealed that it binds in the same pocket as TCA1 (**23**) and forms three hydrogen bonds with Lys134, Ser228, and Trp230.[73]

Tetracycline, an unusual non-covalent DprE1 inhibitor

Wilsey *et al.*,[74] searched for potent non-covalent inhibitors and performed a virtual screen of 4.1 million compounds against DprE1 (PDB 4FDO). Amongst them, only a tetracycline-based compound (**81**) (Figure 13) showed the highest zone of inhibition. This compound showed structural similarity to tetracycline and had an *in-silico* binding affinity of −12.3 kcal/mol. The docking pose analysis revealed that tetracycline binds in the substrate-binding region of the active site of DprE1. The planar shape of tetracycline is accommodated and aligns parallel to the isoalloxazine ring of FAD. Based on the structural similarity search on the compound, it was found that four fused rings and amide functional groups are essential for the high binding affinity. The NH_2 of the free amide group forms a hydrogen bond with Tyr60 and Phe320, while the nitrogen of FAD interacts with adjacent alcohol *via* hydrogen bonding. A compound similar to tetracycline, so work here suggests that tetracycline (**81**) also binds to DprE1 and prevents cell wall formation[74]

Ligand Interaction Analysis of Important DprE1 Inhibitors Deposited in the PDB Server

DprE1 inhibitors with NO_2-aromatic heterocycles6HEZ[23]

The co-crystalized structure of BTZ043 (**9**) with $DprE1_{TB}$was deposited in PDB server with a resolution of 2.30 Å. The ligand is situated in a substrate/inhibitor-binding pocket in front of the isoalloxazine ring of FAD. The nitro-group interacts covalently with Cys387. The hydrophobic pocket (head region, see active site analysis of DprE1) formed around the trifluoromethyl (CF_3) group of BTZ043 (**9**) is covered by various side chains of amino acids, including His132, Gly133, Lys134, Lys376, Phe369, and Asp385. The benzothiazinone ring of BTZ043 (**9**) is accommodated in the trunk region, aligned almost parallel to the isoalloxazine ring of FAD on one side and Val365 and Cys387 (with a covalent bond to the nitro group) on the other side. Gly117 and Trp230 surround the piperazine ring. The spiro-cyclic moiety aligns in the tail region but lacks electron density, accounting for the molecule and protein side-chain flexibility. The spiro-cyclic ring forms Van der Waals interactions with Leu317 and Leu363. Overall, BTZ043 (**9**) is an excellent fit in the active site of DprE1, resulting in nanomolar potency. The PDB 4F4Q (DprE1SM) also co-crystallized with BTZ043 (**9**) (Figure 14A) and had the same pose and interaction within the active site. Other reported PDBs, such as 4PFA, 4P8H, 6G83,[22] 4FDN, 4FDO, 4NCR;[19] 6HF0,[23] 6HF3,[23] 6HFV,[23] and 6HFW[23] have similar interaction patterns, but different co-crystal ligands are bound, which are given in (Table 1).[23]

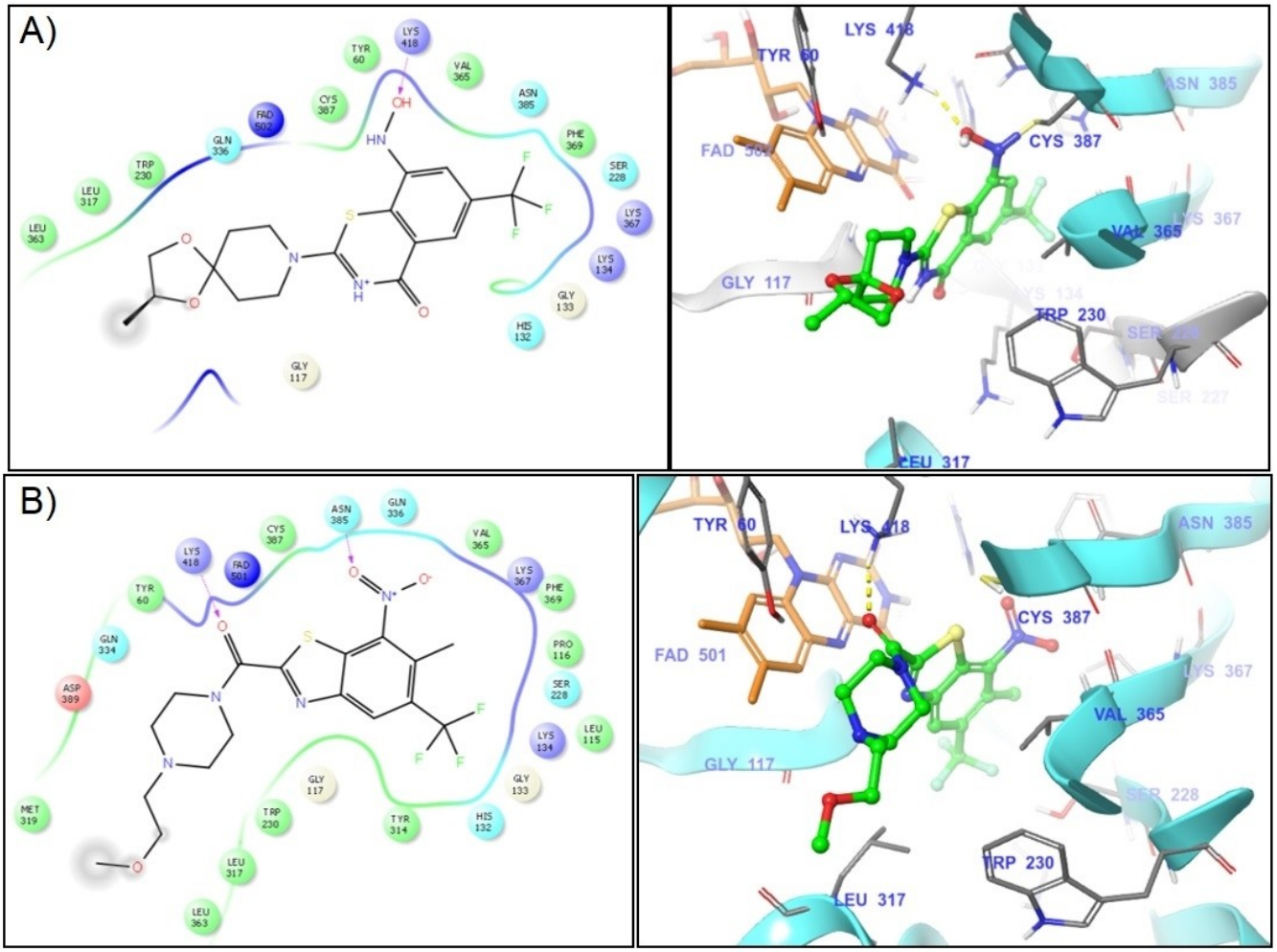

Figure 14. This figure shows the 2D and 3D binding patterns of (A) BTZ043 (9) in complex with DprE1 (PDB 6HEZ[23]) and (B) cBT18 in complex with DprE1 (PDB 4PFD not published). All the ligand-protein interaction diagrams were generated using the MAESTRO-12.5. The carbon atoms of FAD are displayed in orange, while the carbon atoms of the ligand and the amino acid side chains are in green and gray, respectively. Nitrogen, oxygen, and sulfur atoms are colored blue, red, and yellow, respectively. Fluorine atoms are in light green, and amino acid labels are blue.

4PFD

The co-crystallized structure of DprE1TB with cBT18 (**19**) was deposited in the PDB server with a resolution of 2.30 Å. The ligand binds the substrate/inhibitor-binding pocket located in front of the isoalloxazine ring of FAD. The methyl group lies in a hydrophobic pocket in the head region. Although cBT18 contains the same covalent warhead (aromatic NO_2-CF_3) as BTZ043 (**9**), the nitro group does not form a covalent bond with Cys387 due to the presence of a methyl group between the NO_2 and CF_3. Instead, it is stabilized by forming a hydrogen bond with the polar residue Asp385 in the trunk region. The benzthiazole ring is accommodated in the trunk region, but due to an additional methyl group, the nitro group cannot form a covalent bond with Cys387. The carbonyl group of benzthiazole carboxamide creates additional hydrogen bonding with Lys418, thus stabilizing the complex. The piperidine ring is surrounded by Tyr60, Leu317, Gln334, and Trp230, while the aliphatic chain on the piperidine ring is fully exposed to solvent in the tail region. (Figure 14B) shows the details of the interaction between cBT18 and $DprE1_{TB}$. Note that this structure has not been published.[49]

Compounds without aromatic NO_2-CF_3 warhead4 KW5[18]

The X-ray crystal structure of $DprE1_{TB}$ in complex with TCA1 (**23**), solved at a resolution of 2.61 Å, has been deposited in the Protein Data Bank under accession code 4KW5. The analysis of this structure provides detailed insights into the binding mode of TCA1 (**23**), revealing a boomerang-like conformation of the ligand. The thiophene moiety is located in a hydrophobic pocket in the head region. On one side, TCA1's benzothiazole ring is surrounded by an isoalloxazine ring of FAD, and by Val365 and Trp230 on the other side. Hydrogen bonds are formed between the carboxamido group and His132, and between the thiazole-nitrogen of TCA1 (**23**) and Lys418. The

carbamate and phenyl ring of Tyr314 interact via van der Waals forces to stabilize the ligand and develop a positive interaction with Lys134. Both carbonyl groups of the thiophene-3-carbonyl-carbamate form strong hydrogen-bonding interactions with Ser220. While the ligand fits into the active site, the carbamate's benzothiazole and ethyl side chain are exposed to the solvent and lie in the tail region. (Figure 15A) shows that TCA1 (**23**) has several interactions in the active site, and therefore, an increased potency was observed.[18]

4P8C[58]

The crystal structure of the $DprE1_{TB}$-QN127(**7**) complex (PDB 4P8 C) has been determined at a resolution of 1.95 Å, revealing the binding mode of QN127(7) to the substrate/inhibitor-binding domain of $DprE1_{TB.}$ The carboxyquinoxaline ring is situated in front of the isoalloxazine ring of FAD, with the CF_3 group lying in a hydrophobic pocket in the head region. The carboxylate group of QN127 (**7**) and N1 of the quinoxaline forms a hydrogen bond with Lys418 and Tyr60. The substituted benzyl ring aligns with the tail region but is not fully exposed to the solvent, as it is surrounded by Leu363, Trp230, and Leu317. An additional ligand, polypropylene glycol, colored in magenta, is bound in the lower side of QN127 (**7**), as shown in (Figure 15B). Similar interactions are observed in other PDBs, such as 4P8K,[58] 4P8L,[58] 4P8N,[58] 4P8N,[58] 4P8P,[58] 4P8T,[58] and 4P8Y.[58]

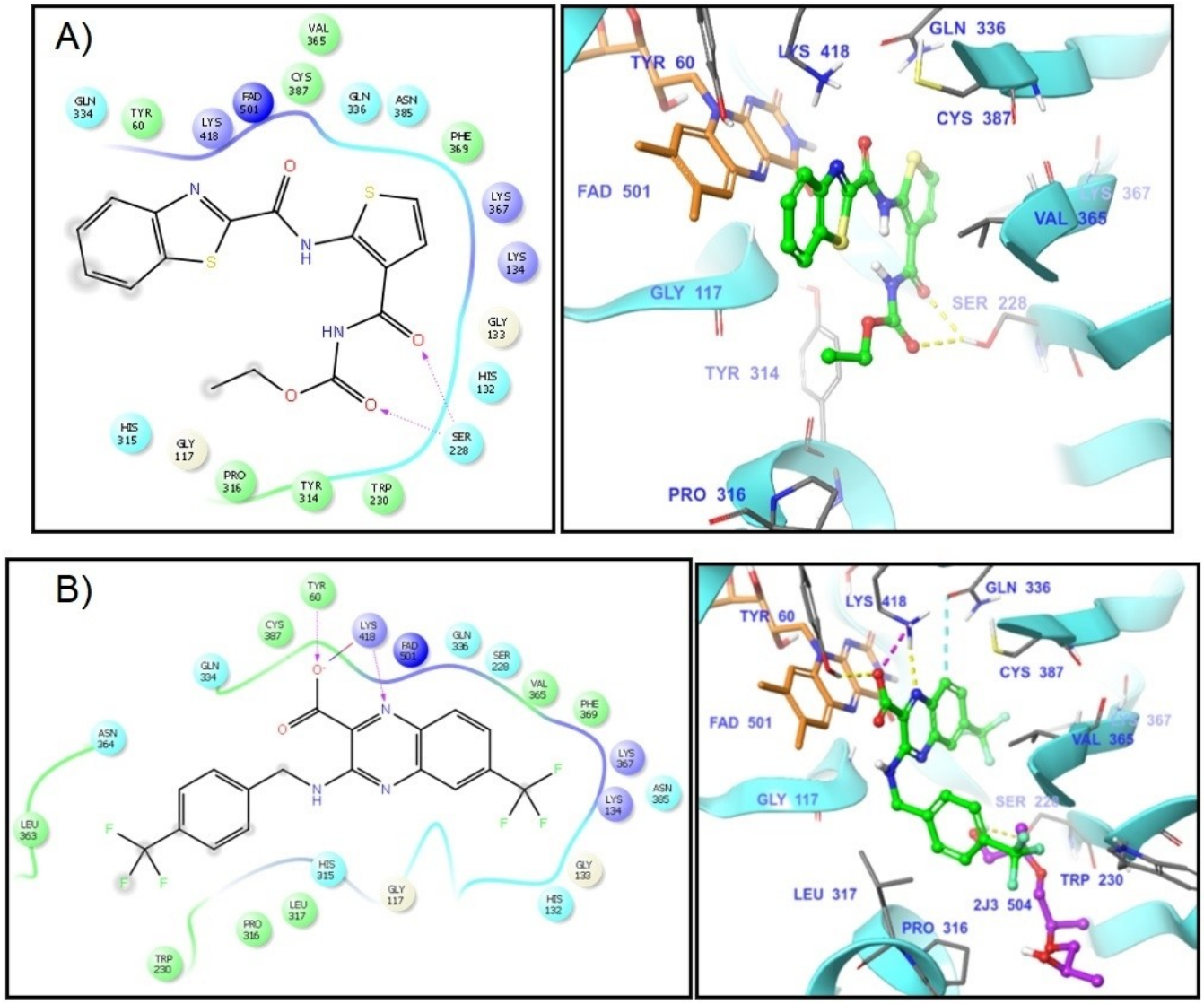

Figure 15. A) 2D and 3D binding pattern of TCA1 in complex DprE1 (PDB 4KW5[18]). **B**) 2D and 3D binding pattern of QN127 (**7**) in complex DprE1 (PDB 4P8C[58]).

Resistance Mechanisms

Resistance mechanisms reported against known anti-TB drugs

Various types of resistance mechanisms have been clinically shown by different kinds of anti-TB drugs. The most common resistance mechanisms against anti-TB drugs include the following: 1) pro-drug activation, as observed for isoniazid, where a mutation within katG encodes for a catalase-peroxidase and prevents the formation of an isoniazid-NAD adduct; 2) mutation within the target (or promoter sequence), for instance, mutations within inhA (enoyl-ACP reductase) for isoniazid; 3) rifampicin resistance develops with mutations in rpoB (codons 507–533, also called the hot spot region) that encode for the ß-subunit of the RNA polymerase, which leads to conformational changes in the enzyme, thus decreasing the affinity towards rifampicin. Rifampicin resistance is considered a surrogate marker for MDR-TB because almost all rifampicin-resistant strains are also resistant to other drugs, and mono-resistance to rifampicin is very rare. Codons 516, 526, and 531 are the most commonly responsible for mutations associated with rifampicin resistance. 4) Ethambutol resistance has been observed with a missense mutation in the embB gene at position 306. 5) Fluoroquinolones develop resistance due to mutations in gyrA or gyrB encoding for DNA gyrase enzyme. The most common mutation was observed at 90 and 94 gyrA genes, but mutations at 74, 88, and 91 have also been reported. 5) Streptomycin resistance is associated with mutations in rpsL and rrs genes that code for ribosomal protein S12 and 16S rRNA, respectively.[4,75]

Resistance mechanism of covalent DprE1 inhibitors

Many DprE1 inhibitors have developed resistance mechanisms in the laboratory, such as covalent inhibitors like benzothiazinone, MTX, and Dinitrobenzamides inhibiting DprE1 by mutations at Cys387 by replacing it with Serine or Glycine.[4,75]

Resistance mechanism of non-covalent DprE1 inhibitors

Several non-covalent inhibitors, such as azaindole, benzimidazole, and 4-aminoquinolone piperidine amides, have shown acquired resistance due to a nucleotide change at Tyr314 to His314.[53–54,57,76] The complex of TCA1 (**23**) and $DprE1_{TB}$ revealed that TCA1 (**23**) was situated in the central cavity of DprE1 in a boomerang-like framework, where the carbamate moiety forms Van der Waals interactions with the phenyl ring of Tyr314, which is essential for the binding of TCA1 (**23**). The importance of this interaction was demonstrated when Tyr314 is mutated to alanine, leading to a TCA1 (**23**) resistant mutant.[18] Similarly, resistance against DprE1 has been observed for 1,4-azaindole (**57**) due to a point mutation that causes an amino acid substitution from Trp314 to His314.[52] This single amino acid change can lead to a loss of affinity for the inhibitor, reducing its effectiveness in inhibiting DprE1. However, benzimidazole (**58**) showed resistance due to the shift from Tyr314 to Ser314 substitution.[54] In the case of quinoxalines (TY36c (20) and QN129 (8)), the carboxylate group forms hydrogen bonds with Lys418 and Tyr60 as well as with Arg325, while two quinoxaline-resistant mutants (G17C and L368P) do not directly interact with quinoxaline inhibitors but lead to conformational changes in the binding pocket.[58]

Analysis of Physicochemical (PC) and ADMET Properties of DprE1 inhibitors

Amado *et al.*[13b] performed a comprehensive analysis of physicochemical descriptors and ADMET properties for 1,519 DprE1 inhibitors reported in the literature between 2009 and April 2022. The analysis revealed that covalent inhibitors showed higher potential as P-gp substrates but had limited CNS penetration. The major predicted isoform involved in metabolizing DprE1 inhibitors was CYP3A4. The study also highlighted the increased cardiovascular toxicity in covalent inhibitors and the mutagenic warnings associated with nitro-aromatic compounds. These findings underscore the importance of considering physicochemical descriptors and ADMET properties during the development of DprE1 inhibitors to ensure their effectiveness and safety.

Conclusions

The increasing number of MDR and XDR TB cases has created a pressing need to discover new anti-TB drugs that are more effective, less toxic, and have shorter treatment durations. DprE1 inhibitors have the potential to provide future anti-TB medications, as DprE1 is a highly druggable target and various chemical scaffolds have shown activity against it, including benzothiazinone, piperazine-benzothiazinone, benzothiazole, benzimidazole, azaindole, pyrimidinetrione, phenylpropanamides, and hydantoin. Most potent compounds differ in structure, but all bind into the substrate/inhibitor-binding region and have diverse types of favorable interactions in the active site's head, trunk, and tail regions. Based on binding site analysis, we observed that the active site of DprE1 is large enough to accommodate larger molecules like polycyclic, macrocyclic compounds, and other two- to four-ring heterocycles with or without covalent warheads. The flexible nature of DprE1's binding site and its association with DprE2 limit its potential for discovering new drugs with improved efficacy. This provides an opportunity for medicinal chemists to examine the DprE1-DprE2 interface closely and discover new molecules that meet the receptor requirements. This requires strong efforts to identify newer compounds that not only exhibit good binding to the target but also have enhanced pharmacokinetic properties to reach the target in sufficient amounts without significant interactions with host proteins. Overall, the availability of diverse ligands and wealth of various crystal structures makes this protein a gold standard target for discovering future anti-TB drugs.

Acknowledgements

The corresponding author acknowledges the support from Science and Engineering Research Board (SERB), New Delhi, India in the form of a SERB International Research Experience (SIRE) award (SIR/2022/000171). Also acknowledges the Director, Shri Govindram Seksaria Institute of Technology and Science, (S.G.S.I.T.S.), 23-Park Road, Indore, Madhya Pradesh (India), for providing sufficient infrastructure facilities for completing this work.

Conflict of Interests

The authors declare no conflict of interest.

Data Availability Statement

The data that support the findings of this study are available from the corresponding author upon reasonable request.

Keywords: DprE1 · arabinogalactan · covalent inhibitors · noncovalent inhibitors · benzothiazinone · tuberculosis

[1] WHO, "*Global tuberculosis report 2019*", can be found under https://www.who.int/tb/publications/factsheet global.pdf?ua=1, **2019**, accessed 02 November 2019.
[2] a) M. A. Espinal, A. Laszlo, L. Simonsen, F. Boulahbal, S. J. Kim, A. Reniero, S. Hoffner, H. L. Rieder, N. Binkin, C. Dye, R. Williams, M. C. Raviglione, *N. Engl. J. Med.* **2001**, *344*, 1294–1303; b) J. L. Khawbung, D. Nath, S. Chakraborty, *Comparative Immunology, Microbiology and Infectious Diseases* **2021**, *74*, 101574.
[3] D. Machado, J. Perdigão, I. Portugal, M. Pieroni, P. A. Silva, I. Couto, M. Viveiros, *Antibiotics* **2018**, *7*, 18.
[4] J. C. Palomino, A. Martin, *Antibiotics* **2014**, *3*, 317–340.
[5] N. Dookie, S. Rambaran, N. Padayatchi, S. Mahomed, K. Naidoo, *The Journal of antimicrobial chemotherapy* **2018**, *73*, 1138–1151.
[6] D. Machado, M. Girardini, M. Viveiros, M. Pieroni, *Front. Microbiol.* **2018**, *9*, 1367–1367.
[7] E. J. Forget, D. Menzies, *Expert Opin. Drug Saf.* **2006**, *5*, 231–249.
[8] a) L. Favrot, D. R. Ronning, *Expert Rev. Anti-Infect. Ther.* **2012**, *10*, 1023–1036; b) G. Piccaro, G. Poce, M. Biava, F. Giannoni, L. Fattorini, *The Journal of Antibiotics* **2015**, *68*, 711–714.
[9] a) R. Singh, S. P. Dwivedi, U. S. Gaharwar, R. Meena, P. Rajamani, T. Prasad, *Journal of Applied Microbiology* **2020**, *128*, 1547–1567; b) K. Duncan, C. E. Barry, *Curr. Opin. Microbiol.* **2004**, *7*, 460–465.
[10] a) A. Bahuguna, D. S. Rawat, *Medicinal Research Reviews* **2020**, *40*, 263–292; b) Y. S. Kwon, B. H. Jeong, W. J. Koh, *Current opinion in pulmonary medicine* **2014**, *20*, 280–286; c) R. Tandon, M. Nath, *Mini-Rev. Med. Chem.* **2017**, *17*, 549–570; d) D. Kumar, B. Negi, D. S. Rawat, *Future Med. Chem.* **2015**, *7*, 1981–2003; e) F. Squeglia, M. Romano, A. Ruggiero, R. Berisio, *Curr. Med. Chem.* **2017**, *24*, 3954–3969; f) J. de Oliveira Viana, H. M. Ishiki, M. T. Scotti, L. Scotti, *Curr. Top. Med. Chem.* **2018**, *18*, 750–758; g) J. L. MD, H. I. Boshoff, C. E. Barry, 3rd, *Curr. Opin. Pharmacol.* **2018**, *42*, 81–94; h) M. Igarashi, *Biosci. Biotechnol. Biochem.* **2017**, *81*, 32–37; i) K. A. Abrahams, G. S. Besra, *RSC Med. Chem.* **2020**, *11*, 1354–1365; j) K. A. Abrahams, G. S. Besra, *RSC Medicinal Chemistry journal* **2020**, *11*, 1354–1365.
[11] E. Fullam, R. J. Young, *RSC Med. Chem.* **2021**, *12*, 43–56.
[12] a) S. M. Batt, C. E. Burke, A. R. Moorey, G. S. Besra, *The Cell Surface* **2020**, *6*, 100044; b) G. Manina, M. R. Pasca, S. Buroni, E. De Rossi, G. Riccardi, *Curr. Med. Chem.* **2010**, *17*, 3099–3108; c) G. S. Shetye, S. G. Franzblau, S. Cho, *Transl. Res.* **2020**, *220*, 68–97.
[13] a) R. V. Chikhale, M. A. Barmade, P. R. Murumkar, M. R. Yadav, *J. Med. Chem.* **2018**, *61*, 8563–8593; b) P. S. M. Amado, C. Woodley, M. L. S. Cristiano, P. M. O'Neill, *ACS Omega* **2022**, *7*, 40659–40681; c) J. Gawad, C. Bonde, *Chemistry Central Journal* **2018**, *12*, 72; d) G. Degiacomi, J. M. Belardinelli, M. R. Pasca, E. De Rossi, G. Riccardi, L. R. Chiarelli, *Applied Sciences* **2020**, *10*, 623; e) S. M. Batt, T. Jabeen, V. Bhowruth, L. Quill, P. A. Lund, L. Eggeling, L. J. Alderwick, K. Fütterer, G. S. Besra, *Proc. Natl. Acad. Sci. USA* **2012**, *109*, 11354–11359.
[14] K. Mikusová, H. Huang, T. Yagi, M. Holsters, D. Vereecke, W. D'Haeze, M. S. Scherman, P. J. Brennan, M. R. McNeil, D. C. Crick, *J. Bacteriol.* **2005**, *187*, 8020–8025.
[15] G. Riccardi, M. R. Pasca, L. R. Chiarelli, G. Manina, A. Mattevi, C. Binda, *Appl. Microbiol. Biotechnol.* **2013**, *97*, 8841–8848.
[16] V. Makarov, G. Manina, K. Mikusova, U. Mollmann, O. Ryabova, B. Saint-Joanis, N. Dhar, M. R. Pasca, S. Buroni, A. P. Lucarelli, A. Milano, E. De Rossi, M. Belanova, A. Bobovska, P. Dianiskova, J. Kordulakova, C. Sala, E. Fullam, P. Schneider, J. D. McKinney, P. Brodin, T. Christophe, S. Waddell, P. Butcher, J. Albrethsen, I. Rosenkrands, R. Brosch, V. Nandi, S. Bharath, S. Gaonkar, R. K. Shandil, V. Balasubramanian, T. Balganesh, S. Tyagi, J. Grosset, G. Riccardi, S. T. Cole, *Science* **2009**, *324*, 801–804.
[17] J. Piton, C. S. Foo, S. T. Cole, *Drug Discovery Today* **2017**, *22*, 526–533.
[18] F. Wang, D. Sambandan, R. Halder, J. Wang, S. M. Batt, B. Weinrick, I. Ahmad, P. Yang, Y. Zhang, J. Kim, M. Hassani, S. Huszar, C. Trefzer, Z. Ma, T. Kaneko, K. E. Mdluli, S. Franzblau, A. K. Chatterjee, K. Johnsson, K. Mikusova, G. S. Besra, K. Fütterer, S. H. Robbins, S. W. Barnes, J. R. Walker, W. R. Jacobs, Jr., P. G. Schultz, *Proc. Natl. Acad. Sci. USA* **2013**, *110*, E2510–E2517.
[19] V. Makarov, B. Lechartier, M. Zhang, J. Neres, A. M. van der Sar, S. A. Raadsen, R. C. Hartkoorn, O. B. Ryabova, A. Vocat, L. A. Decosterd, N. Widmer, T. Buclin, W. Bitter, K. Andries, F. Pojer, P. J. Dyson, S. T. Cole, *EMBO Mol. Med.* **2014**, *6*, 372–383.
[20] S. Landge, A. B. Mullick, K. Nagalapur, J. Neres, V. Subbulakshmi, K. Murugan, A. Ghosh, C. Sadler, M. D. Fellows, V. Humnabadkar, J. Mahadevaswamy, P. Vachaspati, S. Sharma, P. Kaur, M. Mallya, S. Rudrapatna, D. Awasthy, V. K. Sambandamurthy, F. Pojer, S. T. Cole, T. S. Balganesh, B. G. Ugarkar, V. Balasubramanian, B. S. Bandodkar, M. Panda, V. Ramachandran, *Bioorg. Med. Chem.* **2015**, *23*, 7694–7710.
[21] R. Liu, X. Lyu, S. M. Batt, M. H. Hsu, M. B. Harbut, C. Vilchèze, B. Cheng, K. Ajayi, B. Yang, Y. Yang, H. Guo, C. Lin, F. Gan, C. Wang, *Angewandte Chemie (International ed. in English)* **2017**, *56*, 13011–13015.
[22] J. Piton, A. Vocat, A. Lupien, C. S. Foo, O. Riabova, V. Makarov, S. T. Cole, *Antimicrob. Agents Chemother.* **2018**, *62*, e00681–00618.
[23] A. Richter, I. Rudolph, U. Möllmann, K. Voigt, C. W. Chung, O. M. P. Singh, M. Rees, A. Mendoza-Losana, R. Bates, L. Ballell, S. Batt, N. Veerapen, K. Fütterer, G. Besra, P. Imming, A. Argyrou, *Sci. Rep.* **2018**, *8*, 13473.
[24] J. Neres, F. Pojer, E. Molteni, L. R. Chiarelli, N. Dhar, S. Boy-Röttger, S. Buroni, E. Fullam, G. Degiacomi, A. P. Lucarelli, R. J. Read, G. Zanoni, D. E. Edmondson, E. De Rossi, M. R. Pasca, J. D. McKinney, P. J. Dyson, G. Riccardi, A. Mattevi, S. T. Cole, C. Binda, *Sci. Transl. Med.* **2012**, *4*, 150ra121.
[25] H. Li, G. Jogl, *Proteins Struct. Funct. Bioinf.* **2013**, *81*, 538–543.
[26] a) J. C. Sammartino, M. Morici, G. Stelitano, G. Degiacomi, G. Riccardi, L. R. Chiarelli, *Biochem. Biophys. Res. Commun.* **2022**, *607*, 49–53; b) I. Bhutani, S. Loharch, P. Gupta, R. Madathil, R. Parkesh, *PLoS One* **2015**, *10*, e0119771.
[27] S. Chhabra, S. Kumar, R. Parkesh, *ACS Omega* **2021**, *6*, 14430–14441.
[28] S. M. Batt, S. Toth, B. Rodriguez, K. A. Abrahams, N. Veerapen, G. Chiodarelli, L. R. Cox, P. J. Moynihan, J. Lelievre, K. Fütterer, G. S. Besra, *Microbiology* **2023**, *169*.
[29] a) H. Verma, S. Choudhary, P. K. Singh, A. Kashyap, O. Silakari, *Mol. Simul.* **2019**, *45*, 1515–1523; b) F. Kloss, V. Krchnak, A. Krchnakova, S. Schieferdecker, J. Dreisbach, V. Krone, U. Möllmann, M. Hoelscher, M. J. Miller, *Angew. Chem. Int. Ed.* **2017**, *56*, 2187–2191; c) T. Karoli, B. Becker, J. Zuegg, U. Möllmann, S. Ramu, J. X. Huang, M. A. Cooper, *J. Med. Chem.* **2012**, *55*, 7940–7944; d) V. A. M. Makarov, RU), Cole, Stewart T. (Lausanne, CH), Möllmann, Ute (Jena, DE),, Leibniz Institute for Natural Product Research and Infection Biology E. V. (Jena, DE), United States, **2007**; e) Cinicaltrials.gov, "*Phase 2a Study of PBTZ169*", can be found under https://clinicaltrials.gov/ct2/show/NCT03334734, **2017**, accessed 22 May 2023.
[30] a) C. S.-Y. Foo, B. Lechartier, G. S. Kolly, S. Boy-Röttger, J. Neres, J. Rybniker, A. Lupien, C. Sala, J. Piton, S. T. Cole, *Antimicrob. Agents Chemother.* **2016**, *60*, 6451–6459; b) C. Trefzer, M. Rengifo-Gonzalez, M. J. Hinner, P. Schneider, V. Makarov, S. T. Cole, K. Johnsson, *J. Am. Chem. Soc.* **2010**, *132*, 13663–13665.
[31] S. M. Batt, M. Cacho Izquierdo, J. Castro Pichel, C. J. Stubbs, L. Vela-Glez Del Peral, E. Pérez-Herrán, N. Dhar, B. Mouzon, M. Rees, J. P.

Hutchinson, R. J. Young, J. D. McKinney, D. Barros Aguirre, L. Ballell, G. S. Besra, A. Argyrou, *ACS Infect. Dis.* **2015**, *1*, 615–626.
[32] C. Trefzer, H. Škovierová, S. Buroni, A. Bobovská, S. Nenci, E. Molteni, F. Pojer, M. R. Pasca, V. Makarov, S. T. Cole, G. Riccardi, K. Mikušová, K. Johnsson, *J. Am. Chem. Soc.* **2012**, *134*, 912–915.
[33] T. Christophe, M. Jackson, H. K. Jeon, D. Fenistein, M. Contreras-Dominguez, J. Kim, A. Genovesio, J. P. Carralot, F. Ewann, E. H. Kim, S. Y. Lee, S. Kang, M. J. Seo, E. J. Park, H. Skovierová, H. Pham, G. Riccardi, J. Y. Nam, L. Marsollier, M. Kempf, M. L. Joly-Guillou, T. Oh, W. K. Shin, Z. No, U. Nehrbass, R. Brosch, S. T. Cole, P. Brodin, *PLoS Pathog.* **2009**, *5*, e1000645.
[34] R. Liu, V. Krchnak, S. N. Brown, M. J. Miller, *ACS Med. Chem. Lett.* **2019**, *10*, 1462–1466.
[35] M. Brecik, I. Centárová, R. Mukherjee, G. S. Kolly, S. Huszár, A. Bobovská, E. Kilacsková, V. Mokošová, Z. Svetlíková, M. Šarkan, J. Neres, J. Korduláková, S. T. Cole, K. Mikušová, *ACS Chem. Biol.* **2015**, *10*, 1631–1636.
[36] R. Sommer, J. Neres, J. Piton, N. Dhar, A. van der Sar, R. Mukherjee, T. Laroche, P. J. Dyson, J. D. McKinney, W. Bitter, V. Makarov, S. T. Cole, *ACS Chem. Biol.* **2018**, *13*, 3184–3192.
[37] C. Gao, T.-H. Ye, N.-Y. Wang, X.-X. Zeng, L.-D. Zhang, Y. Xiong, X.-Y. You, Y. Xia, Y. Xu, C.-T. Peng, W.-Q. Zuo, Y. Wei, L.-T. Yu, *Bioorg. Med. Chem. Lett.* **2013**, *23*, 4919–4922.
[38] P. Li, B. Wang, X. Zhang, S. M. Batt, G. S. Besra, T. Zhang, C. Ma, D. Zhang, Z. Lin, G. Li, H. Huang, Y. Lu, *Eur. J. Med. Chem.* **2018**, *160*, 157–170.
[39] R. Tiwari, P. A. Miller, S. Cho, S. G. Franzblau, M. J. Miller, *ACS Med. Chem. Lett.* **2015**, *6*, 128–133.
[40] G. Zhang, M. Howe, C. C. Aldrich, *ACS Med. Chem. Lett.* **2019**, *10*, 348–351.
[41] C. Gao, C. Peng, Y. Shi, X. You, K. Ran, L. Xiong, T.-h. Ye, L. Zhang, N. Wang, Y. Zhu, K. Liu, W. Zuo, L. Yu, Y. Wei, *Sci. Rep.* **2016**, *6*, 29717.
[42] L. Xiong, C. Gao, Y.-J. Shi, X. Tao, C.-T. Peng, J. Rong, K.-L. Liu, Q. Lei, Y.-W. Zhang, N.-Y. Wang, L.-T. Yu, *Antimicrob. Agents Chemother.* **2018**, *62*, e02375–02317.
[43] A. Wang, K. Lv, Z. Tao, J. Gu, L. Fu, M. Liu, B. Wan, S. G. Franzblau, C. Ma, X. Ma, B. Han, A. Wang, S. Xu, Y. Lu, *Eur. J. Med. Chem.* **2019**, *181*, 111595.
[44] S. Guo, L. Fu, B. Wang, X. Chen, J. Zhao, M. Liu, Y. Lu, *Biomed. Pharmacother.* **2020**, *131*, 110777.
[45] a) K. Lv, X. You, B. Wang, Z. Wei, Y. Chai, B. Wang, A. Wang, G. Huang, M. Liu, Y. Lu, *ACS Med. Chem. Lett.* **2017**, *8*, 636–641; b) K. Lv, A. Wang, Z. Tao, L. Fu, H. Liu, B. Wang, C. Ma, H. Wang, X. Ma, B. Han, A. Wang, K. Zhang, M. Liu, Y. Lu, *Eur. J. Med. Chem.* **2019**, *179*, 208–217; c) R. Zhang, K. Lv, B. Wang, L. Li, B. Wang, M. Liu, H. Guo, A. Wang, Y. Lu, *RSC Adv.* **2017**, *7*, 1480–1483; d) K. Lv, Z. Tao, Q. Liu, L. Yang, B. Wang, S. Wu, A. Wang, M. Huang, M. Liu, Y. Lu, *Eur. J. Med. Chem.* **2018**, *151*, 1–8.
[46] X. Ma, B. Han, A. Wang, L. Yang, M. Huang, K. Chowdhury, J. Gu, K. Zhang, K. Lv, *RSC Adv.* **2020**, *10*, 14410–14414.
[47] L. Liu, C. Kong, M. Fumagalli, K. Savková, Y. Xu, S. Huszár, J. C. Sammartino, D. Fan, L. R. Chiarelli, K. Mikušová, Z. Sun, C. Qiao, *Eur. J. Med. Chem.* **2020**, *208*, 112773.
[48] R. Tiwari, U. Möllmann, S. Cho, S. G. Franzblau, P. A. Miller, M. J. Miller, *ACS Med. Chem. Lett.* **2014**, *5*, 587–591.
[49] S. Landge, V. Ramachandran, A. Kumar, J. Neres, K. Murugan, C. Sadler, M. D. Fellows, V. Humnabadkar, P. Vachaspati, A. Raichurkar, S. Sharma, S. Ravishankar, S. Guptha, V. K. Sambandamurthy, T. S. Balganesh, B. G. Ugarkar, V. Balasubramanian, B. S. Bandodkar, M. Panda, *ChemMedChem* **2016**, *11*, 331–339.
[50] G. Karabanovich, J. Dušek, K. Savková, O. Pavliš, I. Pávková, J. Korábečný, T. Kučera, H. Kočová Vlčková, S. Huszár, Z. Konyariková, K. Konečná, O. Jand'ourek, J. Stolaříková, J. Korduláková, K. Vávrová, P. Pávek, V. Klimešová, A. Hrabálek, K. Mikušová, J. Roh, *J. Med. Chem.* **2019**, *62*, 8115–8139.
[51] a) J. Roh, G. Karabanovich, H. Vlčková, A. Carazo, J. Němeček, P. Sychra, L. Valášková, O. Pavliš, J. Stolaříková, V. Klimešová, K. Vávrová, P. Pávek, A. Hrabálek, *Bioorg. Med. Chem.* **2017**, *25*, 5468–5476; b) G. Karabanovich, J. Roh, T. Smutný, J. Němeček, P. Vicherek, J. Stolaříková, M. Vejsová, I. Dufková, K. Vávrová, P. Pávek, V. Klimešová, A. Hrabálek, *Eur. J. Med. Chem.* **2014**, *82*, 324–340.
[52] P. S. Shirude, R. Shandil, C. Sadler, M. Naik, V. Hosagrahara, S. Hameed, V. Shinde, C. Bathula, V. Humnabadkar, N. Kumar, J. Reddy, V. Panduga, S. Sharma, A. Ambady, N. Hegde, J. Whiteaker, R. E. McLaughlin, H. Gardner, P. Madhavapeddi, V. Ramachandran, P. Kaur, A. Narayan, S. Guptha, D. Awasthy, C. Narayan, J. Mahadevaswamy, K. G. Vishwas, V. Ahuja, A. Srivastava, K. R. Prabhakar, S. Bharath, R. Kale, M. Ramaiah, N. R. Choudhury, V. K. Sambandamurthy, S. Solapure, P. S. Iyer, S. Narayanan, M. Chatterji, *J. Med. Chem.* **2013**, *56*, 9701–9708.
[53] M. Chatterji, R. Shandil, M. R. Manjunatha, S. Solapure, V. Ramachandran, N. Kumar, R. Saralaya, V. Panduga, J. Reddy, K. R. Prabhakar, S. Sharma, C. Sadler, C. B. Cooper, K. Mdluli, P. S. Iyer, S. Narayanan, P. S. Shirude, *Antimicrob. Agents Chemother.* **2014**, *58*, 5325–5331.
[54] M. M. R, R. Shandil, M. Panda, C. Sadler, A. Ambady, V. Panduga, N. Kumar, J. Mahadevaswamy, M. Sreenivasaiah, A. Narayan, S. Guptha, S. Sharma, V. K. Sambandamurthy, V. Ramachandran, M. Mallya, C. Cooper, K. Mdluli, S. Butler, R. Tommasi, P. S. Iyer, S. Narayanan, M. Chatterji, P. S. Shirude, *ACS Med. Chem. Lett.* **2019**, *10*, 1480–1485.
[55] ClinicalTrials.gov, "*Early Bactericidal Activity of TBA-7371 in Pulmonary Tuberculosis*", can be found under https://clinicaltrials.gov/ct2/show/NCT04176250, **2019**, accessed 22 May 2023.
[56] M. Panda, S. Ramachandran, V. Ramachandran, P. S. Shirude, V. Humnabadkar, K. Nagalapur, S. Sharma, P. Kaur, S. Guptha, A. Narayan, J. Mahadevaswamy, A. Ambady, N. Hegde, S. S. Rudrapatna, V. P. Hosagrahara, V. K. Sambandamurthy, A. Raichurkar, *J. Med. Chem.* **2014**, *57*, 4761–4771.
[57] M. Naik, V. Humnabadkar, S. J. Tantry, M. Panda, A. Narayan, S. Guptha, V. Panduga, P. Manjrekar, L. k. Jena, K. Koushik, G. Shanbhag, S. Jatheendranath, M. R. Manjunatha, G. Gorai, C. Bathula, S. Rudrapatna, V. Achar, S. Sharma, A. Ambady, N. Hegde, J. Mahadevaswamy, P. Kaur, V. K. Sambandamurthy, D. Awasthy, C. Narayan, S. Ravishankar, P. Madhavapeddi, J. Reddy, K. R. Prabhakar, R. Saralaya, M. Chatterji, J. Whiteaker, B. McLaughlin, L. R. Chiarelli, G. Riccardi, M. R. Pasca, C. Binda, J. Neres, N. Dhar, F. Signorino-Gelo, J. D. McKinney, V. Ramachandran, R. Shandil, R. Tommasi, P. S. Iyer, S. Narayanan, V. Hosagrahara, S. Kavanagh, N. Dinesh, S. R. Ghorpade, *J. Med. Chem.* **2014**, *57*, 5419–5434.
[58] J. Neres, R. C. Hartkoorn, L. R. Chiarelli, R. Gadupudi, M. R. Pasca, G. Mori, A. Venturelli, S. Savina, V. Makarov, G. S. Kolly, E. Molteni, C. Binda, N. Dhar, S. Ferrari, P. Brodin, V. Delorme, V. Landry, A. L. de Jesus Lopes Ribeiro, D. Farina, P. Saxena, F. Pojer, A. Carta, R. Luciani, A. Porta, G. Zanoni, E. De Rossi, M. P. Costi, G. Riccardi, S. T. Cole, *ACS Chem. Biol.* **2015**, *10*, 705–714.
[59] O. Balabon, E. Pitta, M. K. Rogacki, E. Meiler, R. Casanueva, L. Guijarro, S. Huss, E. M. Lopez-Roman, Á. Santos-Villarejo, K. Augustyns, L. Ballell, D. B. Aguirre, R. H. Bates, F. Cunningham, M. Cacho, P. Van der Veken, *J. Med. Chem.* **2020**, *63*, 5367–5386.
[60] M. K. Rogacki, E. Pitta, O. Balabon, S. Huss, E. M. Lopez-Roman, A. Argyrou, D. Blanco-Ruano, M. Cacho, C. M. L. Vande Velde, K. Augustyns, L. Ballell, D. Barros, R. H. Bates, F. Cunningham, P. Van der Veken, *J. Med. Chem.* **2018**, *61*, 11221–11249.
[61] J. A. Borthwick, C. Alemparte, I. Wall, B. C. Whitehurst, A. Argyrou, G. Burley, P. de Dios-Anton, L. Guijarro, M. C. Monteiro, F. Ortega, C. J. Suckling, J. C. Pichel, M. Cacho, R. J. Young, *J. Med. Chem.* **2020**, *63*, 2557–2576.
[62] P. Wang, S. M. Batt, B. Wang, L. Fu, R. Qin, Y. Lu, G. Li, G. S. Besra, H. Huang, *J. Med. Chem.* **2021**, *64*, 6241–6261.
[63] N. Hariguchi, X. Chen, Y. Hayashi, Y. Kawano, M. Fujiwara, M. Matsuba, H. Shimizu, Y. Ohba, I. Nakamura, R. Kitamoto, T. Shinohara, Y. Uematsu, S. Ishikawa, M. Itotani, Y. Haraguchi, I. Takemura, M. Matsumoto, *Antimicrob. Agents Chemother.* **2020**, *64*.
[64] a) H. Shimizu, Y. Kawano, S. Ishikawa, Y. Uematsu, T. Shinohara, M. Itotani, Y. Haraguchi, I. Takemura, A. Kaneshige, Y. Nakai, N. Hariguchi, Y. Hayashi, M. Matsumoto, Otsuka Pharmaceutical Co., Ltd., **2016**; b) Y. Nakai, M. Toda, R. Eto, T. Fujii, Otsuka Pharmaceutical Co., Ltd., **2020**; c) F. Valafar, S. J. Modlin, S. M. Radecke, E. Westin, D. Gunasekaran, San Diego State University Research Foundation, **2021**; d) H. Shimizu, Y. Kawano, S. Ishikawa, Y. Uematsu, T. Shinohara, M. Itotani, Y. Haraguchi, I. Takemura, A. Kaneshige, Y. Nakai, N. Hariguchi, Y. Hayashi, M. Matsumoto, Otsuka Pharmaceutical Co., Ltd., **2017**.
[65] ClinicalTrials.gov, "*A Phase 1/2 Trial of Multiple Oral Doses of OPC-167832 for Uncomplicated Pulmonary Tuberculosis*", can be found under https://clinicaltrials.gov/ct2/show/NCT03678688, **2018**, accessed 19 May 2023.
[66] O. Pharmaceutical, "*Otsuka Awarded Grant for Phase 2 Trial Combining Novel Anti-Tuberculosis Compound OPC-167832 with Delamanid and Bedaquiline*", can be found under https://www.otsuka-us.com/news/otsuka-awarded-grant-phase-2-trial-combining-novel-anti-tuberculosis-compound-opc-167832, accessed July 31 2022.
[67] S. Oh, Y. Park, C. A. Engelhart, J. B. Wallach, D. Schnappinger, K. Arora, M. Manikkam, B. Gac, H. Wang, N. Murgolo, D. B. Olsen, M. Goodwin, M.

Sutphin, D. M. Weiner, L. E. Via, H. I. M. Boshoff, *Journal of Medicinal Chemistry* **2018**, *61*, 9952–9965.
[68] V. Makarov, J. Neres, R. C. Hartkoorn, O. B. Ryabova, E. Kazakova, M. Šarkan, S. Huszár, J. Piton, G. S. Kolly, A. Vocat, T. M. Conroy, K. Mikušová, S. T. Cole, *Antimicrob. Agents Chemother.* **2015**, *59*, 4446–4452.
[69] R. Tiwari, P. A. Miller, L. R. Chiarelli, G. Mori, M. Šarkan, I. Centárová, S. Cho, K. Mikušová, S. G. Franzblau, A. G. Oliver, M. J. Miller, *ACS Med. Chem. Lett.* **2016**, *7*, 266–270.
[70] Y. Gao, J. Xie, R. Tang, K. Yang, Y. Zhang, L. Chen, H. Li, *Bioorg. Chem.* **2019**, *85*, 168–178.
[71] E. Lionta, G. Spyrou, D. K. Vassilatis, Z. Cournia, *Curr. Top. Med. Chem.* **2014**, *14*, 1923–1938.
[72] B. C. Whitehurst, R. J. Young, G. A. Burley, M. Cacho, P. Torres, L. Vela-Gonzalez del Peral, *Bioorg. Med. Chem. Lett.* **2020**, *30*, 127192.
[73] P. S. Dube, L. J. Legoabe, A. Jordaan, O. J. Jesumoroti, T. Tshiwawa, D. F. Warner, R. M. Beteck, *Eur. J. Med. Chem.* **2021**, *213*, 113207.
[74] C. Wilsey, J. Gurka, D. Toth, J. Franco, *Comput. Biol. Chem.* **2013**, *47*, 121–125.
[75] Z. S. Bhat, M. A. Rather, M. Maqbool, Z. Ahmad, *Biomed. Pharmacother.* **2018**, *103*, 1733–1747.
[76] a) M. Chatterji, R. Shandil, M. Manjunatha, S. Solapure, V. Ramachandran, N. Kumar, R. Saralaya, V. Panduga, J. Reddy, K. Prabhakar, S. Sharma, C. Sadler, C. Cooper, K. Mdluli, P. Iyer, S. Narayanan, P. Shirude, *Antimicrob. Agents Chemother.* **2014**, *58*; b) P. S. Shirude, R. K. Shandil, M. R. Manjunatha, C. Sadler, M. Panda, V. Panduga, J. Reddy, R. Saralaya, R. Nanduri, A. Ambady, S. Ravishankar, V. K. Sambandamurthy, V. Humnabadkar, L. K. Jena, R. S. Suresh, A. Srivastava, K. R. Prabhakar, J. Whiteaker, R. E. McLaughlin, S. Sharma, C. B. Cooper, K. Mdluli, S. Butler, P. S. Iyer, S. Narayanan, M. Chatterji, *J. Med. Chem.* **2014**, *57*, 5728–5737.
[77] K. Niranjan, R. Srivastava, A. Prakash, A. M. Lynn, *J. Mol. Graphics Modell.* **2021**, *102*, 107770.
[78] G. Zhang, S. Guo, H. Cui, *Molecules* **2018**, *23*, 524.
[79] a) J. Gawad, C. Bonde, *Synth. Commun.* **2019**, *49*, 2696–2708; b) D. Panigrahi, A. Mishra, S. K. Sahu, *SN Applied Sciences* **2020**, *2*, 922.

Manuscript received: February 19, 2023
Revised manuscript received: May 22, 2023
Accepted manuscript online: May 29, 2023
Version of record online: June 29, 2023

REVIEW

DprE1 is a crucial enzyme involved in the cell wall synthesis of *Mycobacterium tuberculosis* and a promising target for antituberculosis drug development. However, the unique structural characteristics for ligand binding and association with DprE2 make developing new clinical compounds challenging. This review provides an in-depth analysis of the structural requirements for both covalent and non-covalent inhibitors, their 2D and 3D binding patterns, as well as their biological activity data in vitro and in vivo, including pharmacokinetic information.

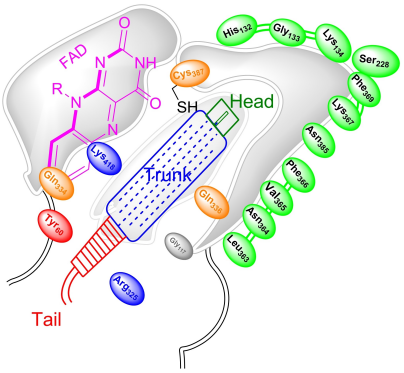

S. Yadav, A. Soni, Dr. O. Tanwar, Dr. R. Bhadane*, Prof. G. S. Besra, Dr. N. Kawathekar*

1 – 32

DprE1 Inhibitors: Enduring Aspirations for Future Antituberculosis Drug Discovery